



Contents lists available at ScienceDirect

Progress in Polymer Science

journal homepage: www.elsevier.com/locate/ppolysci



Polymer nano-foams for insulating applications prepared from CO₂ foaming

C. Forest ^a, P. Chaumont ^a, P. Cassagnau ^{a,*}, B. Swoboda ^b, P. Sonntag ^b

^a IMP@Lyon1, Ingénierie des Matériaux Polymères, CNRS UMR 5223, Université Lyon1, 15 Bd Latarjet, 69622 Villeurbanne, France

^b HUTCHINSON Research Centre, Rue Gustave Nourry - B.P. 31, 45120 Chalette sur Loing, France

ARTICLE INFO

Article history:

Received 17 January 2014

Received in revised form 9 June 2014

Accepted 25 June 2014

Available online xxx

Keywords:

Nano-cell

Nano-foams

CO₂

Thermal conductivity

Polymer foams

Knudsen effect

ABSTRACT

Aspects of the modeling of the thermal conductivity of polymer foams and a CO₂ foaming process for the preparation of micro/nano-cellular polymer materials for insulating applications are reviewed. Generally speaking, the thermal conductivity of polymer foams is higher than that of air. However, it can be expected the Knudsen effect will give nano-cells the thermal insulation properties of aerogels. An analytical model of heat transfer in polymer foams may be used to predict the influence of the foam density and of the cell size on the thermal conductivity of polymer foams. This model derived from aerogel studies suggests the optimal foam density (0.1–0.2 g cm⁻³) and cell size (<100 nm) required to obtain a polymer foam with an effective thermal conductivity lower than that of air.

Foaming processes with CO₂ are reviewed from an experimental perspective. Two different CO₂ processes are generally investigated: (1) a single-stage process where the nucleation is induced by pressure drop quenching after a saturation stage at 'high' temperature under supercritical conditions (foaming process by extrusion, for example) and (2) a two-stage batch process with pressure or thermal quenching to induce cell nucleation and growth after a saturation stage at 'low' temperature under gaseous/supercritical conditions. This review is mainly devoted to the former process. The current challenge in batch CO₂ foaming consists in decreasing the foam densities while keeping cell size lower than 100 nm. For that purpose nucleation must be preferred to increase the cell density up to 10¹⁵ cm⁻³. One way to increase the nucleation is to combine the effects of different nucleating agents to alter the heterogeneous nucleation phenomenon. The nano-structuration of polymers, via block copolymers or nano-fillers, offers a new and original way to fabricate nano-foams with a thermal conductivity lower than that of air. However, some challenges still need to be theoretically and experimentally investigated. On the other hand, if some goals can be met by samples obtained on the lab scale, the scale-up of this foaming process to the pilot and industrial scales is another exciting challenge.

© 2014 Elsevier Ltd. All rights reserved.

Contents

1. Introduction	00
2. Knudsen effect and heat transfers	00
2.1. Heat transfer mechanisms.....	00
2.2. Analytical modeling of heat transfers in aerogels.....	00

* Corresponding author. Tel.: +33 04 72 44 62 08.
E-mail address: philippe.cassagnau@univ-lyon1.fr (P. Cassagnau).

2.2.1.	Conduction via the solid phase	00
2.2.2.	Conduction via the gaseous phase.....	00
2.2.3.	Radiative conductivity	00
2.3.	Implementation in the case of polymer nano-porous materials.....	00
2.3.1.	Conduction via the solid phase	00
2.3.2.	Conduction via the gaseous phase.....	00
2.3.3.	Radiative conductivity	00
2.3.4.	Effective thermal conductivity	00
3.	Supercritical/gaseous CO ₂ foaming process	00
3.1.	CO ₂ sorption during the saturation stage	00
3.1.1.	CO ₂ sorption and diffusion within polymer materials	00
3.1.2.	Effect of CO ₂ solubility on polymer/gas system T _g	00
3.1.3.	Theory on polymer/CO ₂ interactions and CO ₂ -philic polymers.....	00
3.2.	Cell nucleation and growth	00
3.2.1.	Cell nucleation theory	00
3.2.2.	Cell growth mechanisms	00
3.2.3.	Conclusion	00
4.	Fabrication of nano-cellular polymers from nanostructured materials.....	00
4.1.	Foaming of neat block copolymers	00
4.2.	Foaming of polymers nanostructured with nano-fillers	00
4.3.	Foaming of polymers nanostructured with block copolymers	00
4.4.	Conclusion	00
5.	Conclusion and perspectives	00
	Acknowledgements	00
	References	00

1. Introduction

There is significant industrial interest in the development of innovative and efficient materials for thermal insulation applications. Indeed, the energy issues are becoming more and more important because of a possible energy shortage in the future compounded by global warming [1]. Moreover, regulations on thermal insulation in the building trade, aeronautics and gas transport are becoming ever stricter. One of the solutions to these issues is to fabricate materials with very low conductivity.

Thermal conductivity λ is the physical property of a material that describes its capacity to conduct heat, and is directly related to the motion of molecules. It is defined as the speed at which heat spreads through a unit surface, perpendicular to the heat flow direction, per unit of length and temperature. In SI units, thermal conductivity is measured in watts per meter-Kelvin ($\text{W m}^{-1} \text{K}^{-1}$). Table 1 shows the thermal conductivity values (at 300 K, under air pressure) of some solid materials and gas.

Many cellular materials are used in thermal insulation to take advantage of the good insulation capacity of some gases: the conductivity of materials that have low density matches that of the gases: e.g. polystyrene

foams ($\lambda \approx 0.04 \text{ W m}^{-1} \text{ K}^{-1}$) or rigid polyurethane foams ($\lambda \approx 0.03 \text{ W m}^{-1} \text{ K}^{-1}$) [6]. However, in the case of nano-porous foams, the thermal conductivity can become lower than the relevant gas, because of the Knudsen effect that limits the heat conduction via a confined gaseous phase [7]. Nano-cellular foams are widely investigated for many applications, such as molecular separation, catalysis or dielectric applications. Potentially, these materials could be used for thermal insulation, as they have better thermal properties than existing insulation devices.

Fabrication of low density material within which the gas mobility is restricted is a challenge in terms of obtaining a very low thermal conductivity material. Access to such nano-scale structures remains complex via traditional methods, such as selective degradation/etching or gel processes [8–12]. Sub/supercritical CO₂ foaming processes are already used to create polymer micro-foams (cell diameter $\approx 1\text{--}10 \mu\text{m}$), whether in continuous or in batch processes. It may also prove to be a relatively simple and environment-friendly way to create nano-cellular foams, compared with previously cited methods. Considerable effort has been made to optimize the foaming process to decrease the cell size and increase the cell density.

This review focuses on the modeling aspects of foams' thermal conductivity and on the fabrication of micro/nano-cellular polymer materials for insulating applications by means of a CO₂ foaming process.

2. Knudsen effect and heat transfers

The bulk temperature of a gas is a measure of the average kinetic energy of gas molecules as they exchange energy with each other by collision. We denote by τ the average time between collisions and by Λ the mean free path

Table 1
Thermal conductivities at 300 K of some materials and gases.

Material/Gas	Thermal conductivity ($\text{W m}^{-1} \text{K}^{-1}$) $T=300 \text{ K}$
PMMA [2]	0.19
Polystyrene [3]	0.12
Cork [4]	0.04
Air [5]	0.026
Gaseous CO ₂ [5]	0.025

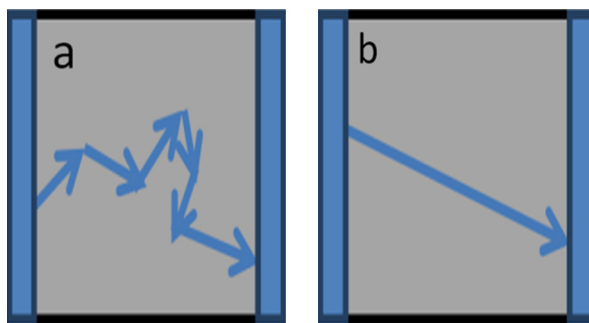


Fig. 1. Diagram of the two heat transport regimes by gas conduction between two walls. (a) Diffusive and (b) ballistic regimes.

(average distance traveled by a moving particle between successive impacts). In the air, the mean free path is about 70 nm at normal temperatures and pressures [13].

When the gas is confined to macro- or micro-cells (with a cell diameter greater than 1 μm), many collisions between gas molecules appear and facilitate heat diffusion. This is called the diffusive regime (see Fig. 1a). If the characteristic dimensions ϕ of the confining cells is lower than Λ , the interactions between gas molecules become scarce and a new transport regime appears: the ballistic regime (see Fig. 1b).

In the case of the ballistic regime, the molecules cross the confining space without being subjected to collisions and do not exchange energy with each other. The heat cannot be diffused by the gaseous phase [14]. Another type of collision becomes predominant: the collision of molecules with the interfaces. The competition between the two types of collisions may be quantified by calculation of the Knudsen number K_n [15]:

$$K_n = \frac{\Lambda}{\phi} = \frac{\eta}{P\phi} \cdot \sqrt{\frac{\pi RT}{2M}} \quad (1)$$

where η : medium viscosity; P : pressure; T : temperature; M : mass of gas molecules; R : gas constant.

The regime that corresponds to a small Knudsen number is well described by Fourier's Law and expresses the appearance of many impacts between gas molecules. When K_n tends to one, the ballistic regime and surface effects are dominant.

This phenomenon could reduce the global thermal conductivity of insulating materials. In order to obtain the optimal conditions and parameters for producing foams with the lowest thermal conductivity possible, the understanding of heat transfer mechanisms within a porous material is essential.

2.1. Heat transfer mechanisms

The heat transfer within cellular materials is composed of four distinct mechanisms [16]:

- conduction via the gaseous phase,
- conduction via the solid phase,
- the radiation phenomenon,

- gas convection, that can be ignored when the cell size is less than 3 mm [17].

Conduction involves a spontaneous thermal transfer from a hot region to a region of lower temperature, without the bulk moving of matter, unlike convection. It can be interpreted as a thermal agitation transfer step by step: a molecule gives part of its kinetic energy to neighboring atoms during collision. It usually responds to the semi-empirical Fourier's law that states that the time rate of heat transfer through a material is proportional to the negative gradient in the temperature, at right angles to that gradient, giving:

$$\vec{\varphi} = -\lambda \overrightarrow{\text{grad}}(T) \quad (2)$$

where λ : material thermal conductivity; T : temperature; $\vec{\varphi}$: heat flow density.

The heat transfer within polymer foams has been studied from different approaches. Collishaw and Evans [18] investigated the following relation for a material made up of spherical cells randomly dispersed within a polymer matrix:

$$\lambda_{gs} = \lambda_g \left(\frac{2V_g + 1 + (\lambda_s/\lambda_g)[2(1 - V_g)]}{(\lambda_s/\lambda_g)(1 - V_g) + 2 + V_g} \right) \quad (3)$$

where λ_{gs} : equivalent thermal conductivity; λ_s : solid phase thermal conductivity; λ_g : gaseous phase thermal conductivity; V_g : volume fraction of gas.

Gibson and Ashby [19] suggested a theoretical model, called the parallel model, for materials with high density of closed cells:

$$\lambda_{gs} = g\lambda_s(1 - V_g) + \lambda_g V_g \quad (4)$$

where g is an efficiency factor that accounts for the tortuous shape of the cell walls and ranges between 1/3 and one.

However, these models do not take into account the gas confinement inside cells and cannot be applied in the case of nano-porous foams.

Other theories have been developed to explain heat transfers, especially for aerogel materials that have very low density and nanometric porosity, giving them a very low thermal conductivity.

2.2. Analytical modeling of heat transfers in aerogels

Silica aerogels are networks of nanometric silica filaments that provide effective porosity with characteristic dimensions from 5 to 71 nm, depending on the fabrication process [20]. Their density can be very low ($\sim 0.1 \text{ g cm}^{-3}$). To date, these materials have the lowest measured thermal conductivities: at room temperature and ambient pressure, they can achieve $0.015 \text{ W m}^{-1} \text{ K}^{-1}$.

An analytical model, initially suggested by Frick and colleagues [21], involves three uncoupled mechanisms to model heat transfers within these materials. The (effective) thermal conductivity λ_{ef} is considered to be the sum of the following components:

- conduction via the solid phase, λ_s ,
- conduction via the gaseous phase, λ_g ,

Table 2

Values of k' according to the material nature of aerogels [22].

Aerogel	k'
Silica	0.39
Resorcinol-formaldehyde	0.57
Melamine-formaldehyde	0.48

- radiative conductivity, λ_r ,

$$\lambda_{ef} = \lambda_s + \lambda_g + \lambda_r \quad (5)$$

Each component is clarified in the following for better understanding of the different heat transfer mechanisms.

2.2.1. Conduction via the solid phase

The contribution λ_s is calculated from an empirical model used to determine the speed of sound in aerogel materials. The values of thermal conductivity obtained are lower than those of the material used because the model takes into account the filaments' tortuosity: the spreading of local excitations to the tortuous network is restricted by the low amount of matter. With this model, we can write:

$$\lambda_s = (1 - \xi) \left[k' \left(\frac{\rho}{\rho_s} \right)^{0.88} \lambda_{s0} \right] \quad (6)$$

where $\xi = 1 - (\rho/\rho_s)$: porosity; λ_{s0} : thermal conductivity of the solid phase; ρ, ρ_s : material and solid network densities; k' : constant that depends on the material nature.

Table 2 gives some values of k' according to the material nature:

2.2.2. Conduction via the gaseous phase

The calculation of λ_g takes into account the Knudsen effect that appears when the porosity size decreases, involving the Knudsen number:

$$\lambda_g = \xi \frac{\lambda_{g0}}{1 + 2aK_n} \quad (7)$$

where ξ : porosity; λ_{g0} : thermal conductivity of the gas; K_n : Knudsen number; a : constant that depends on the gas nature [22].

The parameter a is approximately equal to the accommodation coefficient of the gas with the walls and is between zero and one [21].

2.2.3. Radiative conductivity

The radiation contribution can be written as follows:

$$\lambda_r = \frac{16n^2\sigma T^3}{3\rho(K_s/\rho_s)} \quad (8)$$

where n : refractive index of the aerogel (~ 1); σ : Boltzmann constant $= 5.67 \times 10^{-8} \text{ W m}^{-2} \text{ K}^{-4}$; T : temperature; ρ, ρ_s : material and solid network densities; K_s : average Rosseland extinction coefficient of the solid phase.

2.3. Implementation in the case of polymer nano-porous materials

Eqs. (5)–(8) can be used to estimate the effective thermal conductivity of polymer foams, depending on their density and their average cell size.

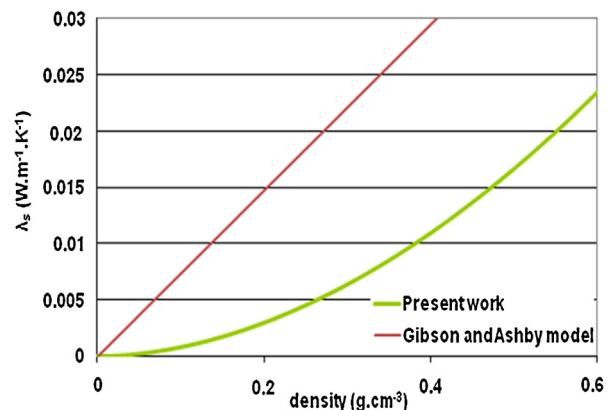


Fig. 2. Theoretical λ_s as a function of polystyrene foam density ($k' = 0.6$) compared with Gibson and Ashby's model ($g = 2/3$) [19].

We study the case of a polystyrene solid skeleton, with a bulk density of 1.087 g cm^{-3} and a thermal conductivity of $0.12 \text{ W m}^{-1} \text{ K}^{-1}$ at 300 K [3]. The polystyrene has a lower thermal conductivity than usual polymers. This means the calculated values of conductivity will give an lower limit for a polymer foam.

2.3.1. Conduction via the solid phase

There are no data concerning the value of k' for polystyrene. A value of 0.6, used in the calculation of the conductivity of organic aerogels, has therefore been chosen. With Eq. (6), λ_s can be plotted according to the foam density (see Fig. 2). Note that the increase of the density causes increased conduction via the solid phase. However, the tortuosity of aerogel filaments is more important than with polymer foams. Gibson and Ashby [19] calculated the contribution of the conduction through the solid phase of a closed-cell polystyrene foam using Eq. (4) with an efficiency factor value of $2/3$. This contribution is reported in Fig. 2 as a function of foam density. It appears to be much higher than in the case of aerogel material. Moreover, even with the lowest efficiency factor value ($1/3$), higher λ_s values are obtained for the Gibson and Ashby model for foam densities lower than 0.55 g cm^{-3} . This confirms that the model underestimates the conduction via the solid phase.

2.3.2. Conduction via the gaseous phase

Air is chosen for the simulation as the gas inside the foam ($\lambda_{g0} = 0.025 \text{ W m}^{-1} \text{ K}^{-1}$, $\Lambda = 70 \text{ nm}$). The maximum value of a is used, that is to say unity, given that $a \approx 1$ for air [22]. With Eq. (7), λ_g is plotted as a function of the foam density and the average cell size Φ (see Fig. 3).

λ_g linearly decreases with the increase of the foam density. Moreover, the more the cell size decreases, the lower the thermal conductivity because the Knudsen effect is taken into account in the calculation.

2.3.3. Radiative conductivity

In the case of a polystyrene aerogel, K_s/ρ_s is $47.8 \text{ m}^2 \text{ kg}^{-1}$ at 300 K [22]. With Eq. (8), the radiative contribution to the thermal conductivity is plotted for $T = 300 \text{ K}$ as a function of the foam density (see Fig. 4).

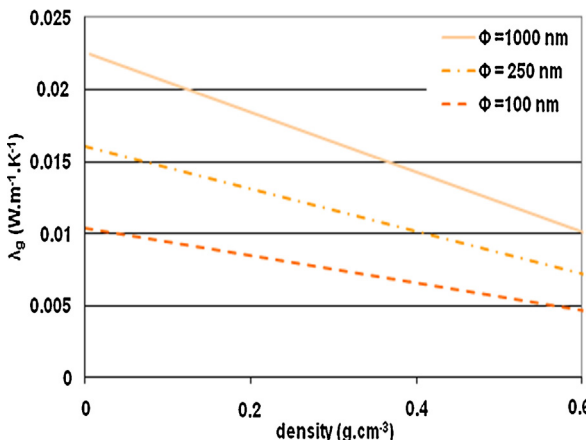


Fig. 3. Theoretical λ_g as a function of polystyrene foam density and cell size.

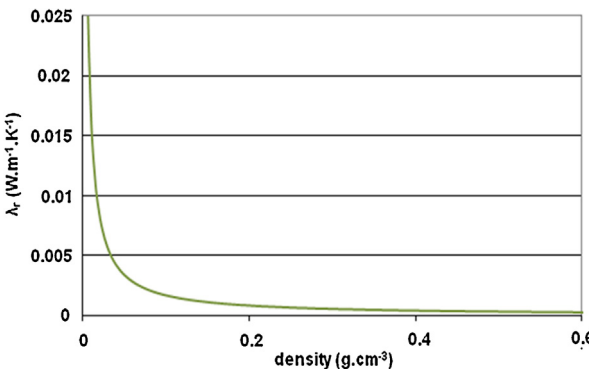


Fig. 4. Theoretical λ_r as a function of polystyrene aerogel density – $T=300$ K.

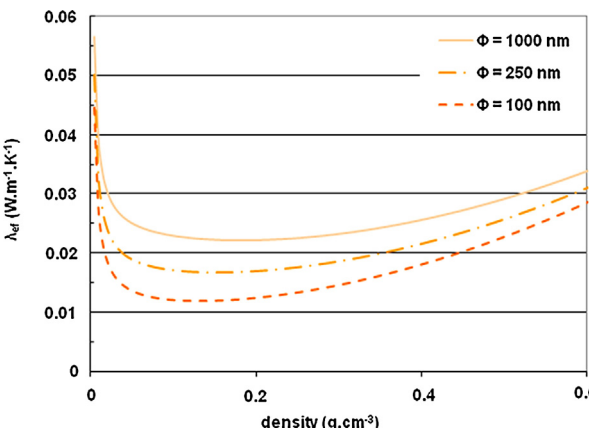


Fig. 5. Theoretical effective thermal conductivity of polystyrene foam as function of foam density and cell size ($T = 300$ K).

2.3.4. Effective thermal conductivity

The effective thermal conductivity obtained from the addition of the different contributions is plotted as a function of the foam density in Fig. 5. It must be remembered that the present model underestimates the conductivity values of the solid and gaseous phases. Consequently, this model provides only qualitative estimates. However, it can

Table 3

Theoretical effective thermal conductivity of equivalent polystyrene foam compared with experimental data for PEI foams from Sundaram and Li's study [25], considering PEI polymer density: 1.28 g cm⁻³ [26].

PEI nano-foams (Sundaram and Li [25])	Effective thermal conductivity (W m ⁻¹ K ⁻¹)	
	Experiments	Aerogel Model (present work)
$\Phi = 260$	0.019	0.020
$\Phi = 240$	0.016	0.018
$\Phi = 86$	0.015	0.013

be useful to determine the optimum density range to obtain the lowest thermal conductivity values. According to the latter, the lowest thermal conductivity can be obtained when the foam density is lower than 0.2 g cm⁻³. Below a density value of 0.1 g cm⁻³, the radiative contribution is no longer negligible. Moreover, the foam must have an average cell size lower than 1 μm to obtain better thermal properties.

The optimum and theoretical cell density can then be calculated as follows (considering spherical cells):

$$d_{\text{cell}} = \frac{3}{4\pi r^3} \left(1 - \frac{\rho}{\rho_s}\right) \quad (9)$$

where ρ, ρ_s : foam and solid phase densities; r : average cell radius.

In the case of polystyrene foam with a density of 0.1 g cm⁻³ and 100 nm diameter cells, the obtained cell density is about 1.5×10^{15} cm⁻³. However, this result represents the final cell density at the end of the foaming process and not the initial cell concentration before the cell expansion. The following equation gives the cell density of original un-foamed material d_0 [23]:

$$d_0 = \frac{d_{\text{cell}}}{1 - V_f} \quad (10)$$

where V_f is the void fraction = $1 - \rho/\rho_s$ [24].

In this case, the cell density d_{cell} of 1.5×10^{15} cm⁻³ of the foamed polymer corresponds to a cell density d_0 of the original preformed material of 1.6×10^{16} cm⁻³. In the following cited studies, a distinction is made between d_{cell} and d_0 . Indeed, some studies only refer to cell density d_{cell} . In these cases, and if data are available, d_0 will be calculated to compare study results.

When the foam density is higher than 0.5 g cm⁻³, with an average cell size of 100 nm, the thermal conductivity of the air is reached. If the polystyrene matrix is replaced by a PMMA matrix in this model ($d = 1.19$ g cm⁻³, $\lambda = 0.2$ W m⁻¹ K⁻¹ at 300 K [2]), the thermal conductivity will increase: a foam with a density of 0.6 g cm⁻³ would have a thermal conductivity of 0.035 W m⁻¹ K⁻¹.

Many approximations have been made in calculations (initially used for aerogel materials). This model only estimates the influence of the foam density and cell size on the thermal conductivity of polymer foams. However, effective thermal conductivities of polyetherimide (PEI) foams (produced in a batch CO₂ foaming process), as by Sundaram and Li [25], approach theoretical values (for an equivalent polystyrene foam in terms of micro/nanostructure). More precisely, Table 3 gives the theoretical effective thermal

conductivities for polystyrene foams of the same density and cell size as PEI foams. Even though the polymer matrices are different, theoretical and experimental values evidently remain close. This excellent agreement could be fortuitous because of the qualitative nature of the model. However, the results show the conditions in terms of both cell and foam densities that must be met for a dominant Knudsen effect.

With this qualitative model, and as reported in the literature [27], the fabrication of super-insulating materials ($\lambda < 0.025 \text{ W m}^{-1} \text{ K}^{-1}$) requires polymer foam with low density ($0.1\text{--}0.2 \text{ g cm}^{-3}$), to limit the conduction via the solid phase, and with a cell diameter lower than 100 nm to reduce the conduction via the gaseous phase.

3. Supercritical/gaseous CO_2 foaming process

As suggested in Section 1, sub/supercritical CO_2 foaming processes could be expected to produce such materials. Microcellular foaming processes, initially used to reduce plastic materials' weight and cost, appeared in the 1980s in the United States [28]. The aim of this development was to fabricate micro-cellular materials conserving the initial mechanical and thermal properties of polymers. Many polymers, such as PVC, polycarbonate, PMMA and PET can be foamed by this process. The produced foams, called micro-cellular materials, have cells with diameters from 1 μm to hundreds of micrometers [28]. However, such foaming processes can be optimized and adapted to more complex polymer systems, to obtain nano-cellular materials with an average cell size of about 100 nanometers. The CO_2 foaming process facilitates the production of polymer foams without using (an additional) solvent and is suitable for industry in batch or continuous process [29,30]. The batch process will be more precisely discussed in this review. It is divided into two distinct stages.

First, polymer plaques or films are placed in a pressure vessel, pressurized with CO_2 until gas saturation is reached. During this stage, the injected CO_2 could be in a gaseous or supercritical state, the latter being easily accessible with a critical point at 31.6°C for a pressure of 7.38 MPa [31]. Rapid pressure or temperature quenching is then applied to change the solubility of the gas within the material, causing gas supersaturation and allowing cell formation. In the first case, the foams are directly recovered at the end of the pressure quenching. In the case of nucleation by thermal destabilization, samples are recovered after a slow pressure drop rate and heated by transfer to a temperature-controlled liquid bath to induce foaming. These two stages are detailed below in order to highlight the physical phenomena occurring in the material during the foaming process.

3.1. CO_2 sorption during the saturation stage

During the saturation stage, a pressure gradient at the surface of a polymer sheet induces two phenomena: the dissolution and the molecular diffusion of the gas within the polymer sheet. The latter is the slower one and therefore the more kinetically determining. These phenomena have been widely investigated for polymer/ CO_2 systems

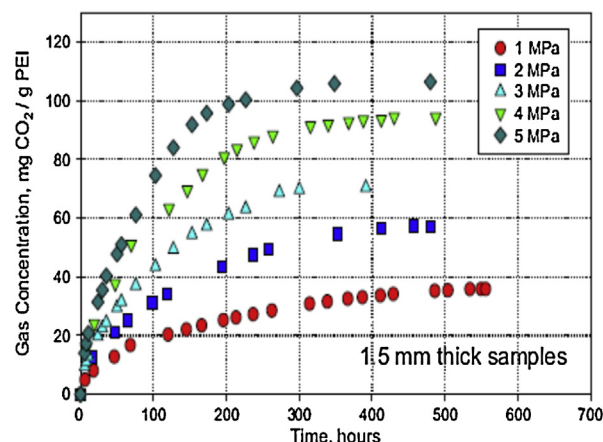


Fig. 6. CO_2 uptake per PEI gram as a function of sorption time and pressure at 21°C [34]. Copyright 2009. Reproduced with permission from Elsevier Ltd.

because of the significant development of polymer blending and processing with pressurized CO_2 [32].

3.1.1. CO_2 sorption and diffusion within polymer materials

The solubility quantifies the absorbed gas content within material in contact with a gaseous phase. At a given temperature, the dissolved gas concentration C depends on the pressure P through the following equation [33]:

$$C = S(C)P \quad (11)$$

where S is the gas solubility.

The influence of the gas pressure on the CO_2 uptake has been studied by Miller and colleagues [34] for the case of gas sorption in polyetherimide (PEI). Polymer plaques (1.5 mm thick) were placed in a pressure vessel at room temperature. During saturation, samples were periodically removed from the pressure vessel, weighed on a high precision balance and then promptly repressurized. Fig. 6 represents the CO_2 uptake per PEI gram according to the pressure and sorption time. It can be seen that the increasing pressure causes an increase in the maximum CO_2 uptake.

Gas solubility S is also dependent on the process temperature, as follows [35,36]:

$$S = S_0 e^{-\Delta H_s/RT} \quad (12)$$

where S_0 : pre-exponential factor; ΔH_s : activation energy for sorption (negative); R : gas constant; T : temperature.

As ΔH_s is negative, an increase in the temperature causes a decrease in gas solubility [37]. Vitoux and colleagues [38] highlighted the sorption temperature influence of the CO_2 uptake of poly(ethylene glycol) samples and showed that a temperature increase from 40°C to 150°C halves sample CO_2 uptake for saturation pressures between 5 and 15 MPa. Indeed, when the temperature increases, the gas is less and less disposed to remain dissolved within materials, in accordance with the laws of thermodynamics.

Since the nano-cell formation process requires fully saturated polymers in most cases, the CO_2 uptake is a key

parameter. To that end, the sorption time has to be sufficient to reach polymer/gas equilibrium and is dependent on gas diffusion within the polymer.

The time evolution of the gas concentration profile can also be described by Fick's classical law as follows:

$$\frac{\partial C}{\partial t} = \nabla \cdot D_{12} \nabla C \quad (13)$$

where D_{12} is the mutual binary diffusion coefficient.

The mutual binary diffusion coefficient D_{12} depends on the volume fraction of dissolved CO_2 [39] but also on the average hole free volume within the polymer/ CO_2 system [40,41]. According to the free volume theory, the temperature, and thus local thermal expansions, induces solvent diffusion variations in the polymer [42,43]. Naito and colleagues [44] used the free volume theory to highlight the pressure effect on the gas diffusion within a polymer material. According to them, when a polymer material is subjected to a high gas pressure, the polymer chains tend to become closer and restrain the free volume. Nevertheless, at the same time the gas concentration within the material increases, causing an increase in the free volume. They suggest the following relation that takes into account these two effects for a given temperature:

$$D(P, C) = D_0 e^{\beta P + \alpha C} \quad (14)$$

where D_0 : pre-exponential factor; β : negative term related to the density increase of the polymer matrix; α : positive term related to the increase of the gas concentration within the polymer matrix.

The glass transition corresponds to increasing the free volume in the polymer/ CO_2 system and improves the solvent diffusion [45]. In the same way, if the addition of a solvent leads to an increasing in the free volume of the system, the glass transition appears at a temperature lower than the polymer T_g [43,46].

3.1.2. Effect of CO_2 solubility on polymer/gas system T_g

In the case of glassy polymer/ CO_2 systems, the polymer is actually plasticized by CO_2 , resulting to a lower glass transition temperature T_g . The plasticization phenomenon is highlighted in Fig. 7, for a PEI sample: the pressure increasing during the saturation stage causes the decreasing of the T_g . More generally, these curves can be used to optimize the foaming process as they allow us to determine the state (glass/rubber) of a polymer/ CO_2 system after the saturation stage.

Several techniques are described in the literature to obtain T_g variations of polymer/gas systems according to their CO_2 uptake, such as DSC experiments at ambient pressure [47], creep compliance [48], dielectric relaxation [49] or X-ray diffraction [50].

However, for Zhang and Handa [51], the thermodynamic state of a polymer/gas system is not always clearly defined with these methods. Especially, in DSC analysis the temperature variation in the cell during the analysis can cause CO_2 uptake variations that modify the state of the polymer/gas system. Zhang and colleagues developed a stepwise temperature-and pressure-scanning thermal analysis method to measure the T_g of a gas polymer system, keeping samples at a thermodynamic equilibrium

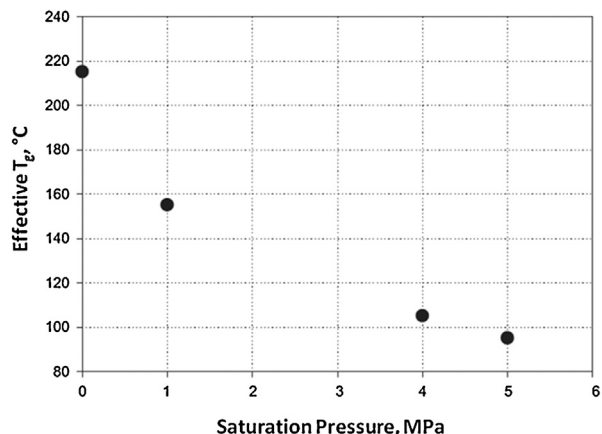


Fig. 7. PEI sample T_g as a function of the CO_2 pressure during the saturation stage [34]. Copyright 2009. Reproduced with permission from Elsevier Ltd.

[52,53]. Indeed, the thermodynamic equilibrium within a polymer/gas system is reached between each step of 15 minutes. This technique consists in carrying out, for a given gas pressure, stepwise temperature jumps and measuring the heat capacity C_p (peak area value). The latter is then plotted as a function of temperature (average temperature between each step), to determine the glass transition from the variation of the observed slope.

Thermodynamic models were also developed to predict the effect of CO_2 uptake on the glass transition. Some refer to the free volume variation within polymer material during the plasticization [45], such as the Doolittle model [54] based on the variation of the polymer/gas viscosity η and on the WLF equation [46]. Chow [55] suggests a model involving the molecular weights of the components and gas uptake to give:

$$\ln \left(\frac{T_g}{T_{g0}} \right) = \psi[(1 - \theta)] \ln(1 - \theta) + \theta \ln \theta \quad (15)$$

$$\text{with } \theta = \frac{\omega/MW_1}{z(1 - \omega)/MW_2} \quad \text{and} \quad \psi = \frac{zR}{MW_2 \Delta C_p}$$

where T_{g0} : glass transition temperature of the polymer; T_g : glass transition temperature of the polymer/gas system with a gas mass fraction ω ; MW_1 , MW_2 : weight-average molecular weight of solvent and polymer, respectively; ΔC_p : variation of the heat capacity of polymer during the glass transition; R : gas constant; Z : coordination number (equal to 1 or 2 in Chow model); ω : gas mass fraction.

The glass transition temperature of some polystyrene/ CO_2 systems is well predicted by this model. However, in the case of PMMA/ CO_2 systems, Handa and colleagues [35] showed that the predicted decrease of the T_g is much lower than the measured value, with a temperature difference of 50 °C and a gas uptake of 11 wt%. In the authors' opinion, this poor correlation is because of strong interactions between the gas molecules and polymer that are not taken into account in the model.

Dong Hwang and Woon Cha [56] made the same observation for ABS/ CO_2 systems. They used a second model, the

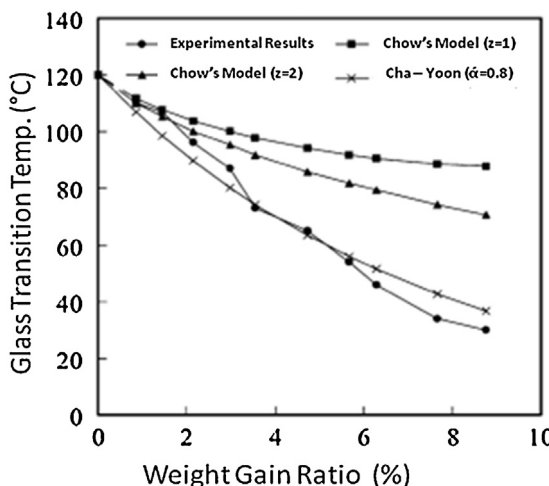


Fig. 8. T_g of ABS samples as a function of CO_2 uptake – comparison between theoretical results and measurements [56]. Copyright 2002. Reproduced with permission from Elsevier Ltd.

Cha-Yoon model [57] that takes into account the polymer density:

$$T_g = T_{go} e^{-(M_w)-(1/3)(\rho_s)-(1/4)\alpha'\omega} \quad (16)$$

where T_{go} : glass transition temperature of the polymer; T_g : glass transition temperature of the polymer/gas system with a gas mass fraction ω ; M_w : weight-average molecular weight of the polymer; ρ_s : polymer density; α' : constant, depending on the polymer/gas system; ω : gas mass fraction.

By varying the α' , depending on the polymer nature (e.g., 7 for PS/ CO_2 system and 8 for ABS/ CO_2 system), they obtained good correlations between theoretical and experimental results (see Fig. 8 for the ABS/ CO_2 system).

This model has also been used for PMMA/ CO_2 systems in Yoon and Cha's study [57] (with $\alpha' = 3$). The latter highlights a drastic decrease of the glass transition temperature that appears for CO_2 uptakes lower than 2 wt%, with the largest decrease of 50 °C. However, such a dramatic variation of T_g has not been observed in other studies. Condo and Johnston [58] predicted, in accordance with experimental results, an equivalent glass transition temperature decrease for a CO_2 uptake of 7.5 wt%, using lattice fluid theory. This result approaches Handa and colleagues' results [35], in terms of CO_2 uptake effect on glass transition temperature. However, even though investigated PMMAs in these different studies have similar initial glass transitions, it is shown that PMMA/ CO_2 systems behavior differ depending on the initial PMMA material and thus limit predictions to specific cases.

In some polymer/gas systems, the relationship between the saturation pressure and the polymer/ CO_2 state also depends on the temperature. Indeed, a retrograde path is observed, and subsequently, two glass transitions are detected under a constant pressure. According to Handa and Zhang [52], this relates to polymer/gas systems near their critical point. This phenomenon can be observed by DSC analysis, solubility tests [35] and also in situ measurements of creep compliance [58,59]. The higher

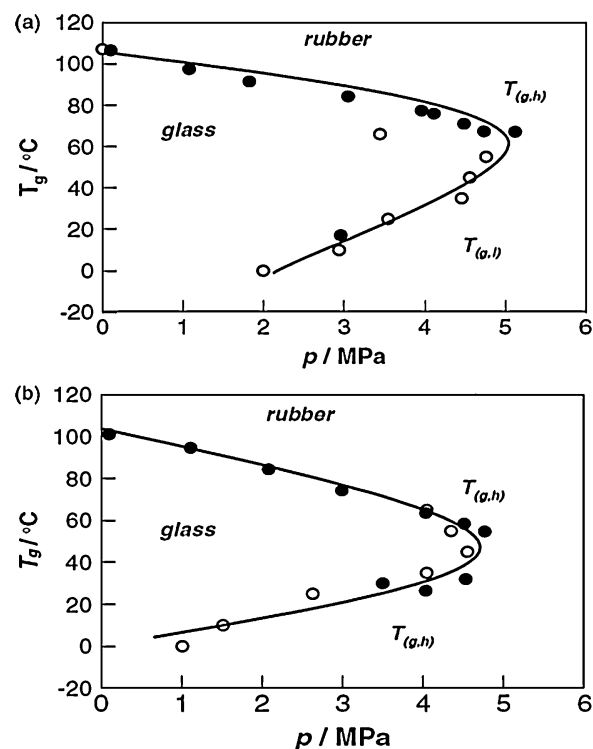


Fig. 9. T_g of (a) PMMA/ CO_2 and (b) ABS/ CO_2 systems as a function of saturation pressure [53]. Copyright 2006. Reproduced with permission from the Society of the Chemical Industry.

T_g corresponds to the CO_2 -plasticized polymer, near the T_g of the neat polymer. The second one occurs at much lower temperatures because of the high CO_2 uptake of the sample: at 'low' temperatures, the gas solubility increases within polymer material, causing the plasticization of the latter. When the temperature increases, the gas solubility quickly decreases and causes the appearance of a second T_g .

This phenomenon has been studied particularly in PMMA/ CO_2 systems [53,56,60] (see Fig. 9a). Indeed, knowledge of glass transition variations allows us to optimize the foaming process of PMMA, that has been widely investigated because of its good insulating properties against the heat, noise and electricity of PMMA foams [61,62]. This behavior also appears for ABS/ CO_2 systems (see Fig. 9b). In both cases, for saturation pressures higher than 5 MPa, polymer/ CO_2 systems would be in a rubbery state.

However, this retrograde behavior has been the subject of debate. Dutriez and colleagues [63] measured glass transition temperature of PMMA/ CO_2 systems using a quartz crystal resonator and showed that a single glass transition appears for saturation pressures between 5 and 25 MPa. Moreover, the latter seems to be constant in this pressure range and close to 10 °C.

Finally, during the foaming process, the gas solubility, and thus the polymer/ CO_2 state, will depend on the polymer nature and its affinity with CO_2 . The effect of polymer/gas interactions acts during the saturation stage in terms of CO_2 uptake but also during the nucleation stage on the polymer plasticization, and thus on the foaming

temperature [64]. In the last thirty years, the latter has been widely studied in the development of new supercritical CO₂ processes for molecule extraction, chromatography or reaction environment [65].

3.1.3. Theory on polymer/CO₂ interactions and CO₂-philic polymers

For any solute/solvent system, the solubility depends on interactions between the two substances. The Flory–Huggins interaction parameter χ is often used and calculated to evaluate the solute/solvent affinity [66]. It is proportional to the term $(\delta_1 - \delta_2)^2$, with δ_1 and δ_2 the solubility parameters of components 1 and 2. The solubility between components increases when solubility parameters are close. Therefore, the miscibility can be estimated by calculating solubility parameters δ . Hildebrand and Scott [67] propose a model based on the calculation of cohesive energy density of the solute/solvent system, such as that in the expression:

$$\delta = \left(\frac{\Delta E}{V} \right)_T^{0.5} \approx \left(\frac{\partial E}{\partial V} \right)_T^{0.5} = \left(T \left(\frac{\partial P}{\partial T} \right)_V - P \right)^{0.5} \quad (17)$$

where $\Delta E/V$: cohesive energy density; T : temperature; P : internal pressure.

This model can be applied to polymer/CO₂ systems with the ideal gas law. Williams and colleagues [65] detailed this principle more precisely and showed that supercritical CO₂ has a higher solubility parameter than gaseous CO₂ and is near those of hydrocarbon chains ($\sim 10 \text{ MPa}^{1/2}$) [68,69]. Strauss and D'Souza [69] showed for a PS/CO₂ system that the condition $\delta_1 - \delta_2 < 1$ required to ensure good gas solubility, would require a saturation pressure of 90 MPa at 80 °C. However, many studies show that CO₂ molecules are partially soluble in polystyrene matrix (more than 13 wt% with saturation pressures lower than 20 MPa [70,71]). This is because the model does not take into account the specific chemical interactions.

Another model, proposed by Hansen and widely used for polymers, is based on interaction distribution in three contributions [72]. According to this treatment, δ can be decomposed as follows:

$$\delta^2 = \delta_d^2 + \delta_p^2 + \delta_h^2 \quad (18)$$

where δ_d : dispersion component; δ_p : polar component; δ_h : hydrogen-bonding component.

These components can be theoretically calculated from the contributions of their chemical groups, that can be found in the literature [73]. Although CO₂ does not have a permanent dipole, the contribution of quadrupole moments in interactions is significant and leads to positive values of δ_p and δ_d in the Hansen model [65]. These results highlight the limitations of this model. Like the Hildebrand and Scott model, it does not take into account specific chemical interactions that improve gas solubility in polymers [74].

The gas sorption behavior is therefore different from one polymer to another depending on the polymer nature, even though they have the same T_g (for example, PMMA and PS). This implies that different molecular compositions of

polymers can lead to different interactions with CO₂. The solubility of fluorinated polymers and block copolymers in compressed CO₂ has been widely investigated [75,76] because of the significant chemical interactions between fluorine-containing polymers and CO₂. These interactions may be of a Lewis acid/base nature. Indeed, the fluorine atom acts as a Lewis base with the electron-deficient carbon of CO₂. In parallel, hydrogen atoms near the fluorine have an induced positive charge and interact with gas oxygen atoms as Lewis acids [77]. Cooper [78] also put forward the hypothesis of weak complex formation between fluoropolymers and CO₂. These interactions increase the gas solubility in fluoropolymers.

Some silicone-based polymers can also be considered as CO₂-philics. However, this seems to be rather the result of the polymer chains' flexibility [79,80]. According to Kirby and McHugh [81] and Nalawade and colleagues [82], CO₂ solubility in poly(dimethyl-) and poly(phenylmethyl-) siloxane is because the free volume fraction is higher than those of other polymers.

Although less CO₂-philic than fluorine- or silicone-based polymers, acrylate and acetate polymers can be cited because of strong interactions between their carbonyl groups and CO₂. In particular, PMMA has been widely studied for its CO₂-philic behavior compared with polyolefins or polystyrene. This affinity is explained by carbonyl group/gas interactions: as regards fluoropolymers, Lewis acid/base interactions appear and increase the gas solubility [69]. These interactions, for PMMA, cellulose acetate and vinyl acetate, have been analyzed by Fourier transform infrared spectroscopy (FT-IR) [83,84]. Kazarian and colleagues [71] worked on the normal vibration mode ν_2 (bending) of CO₂ near 660 cm⁻¹ to study PMMA/CO₂ interactions. In the presence of PMMA macromolecules, the corresponding band splits in two peaks at 662 and 654 cm⁻¹. This splitting is attributed to carbonyl group/gas interactions [82] and does not appear with polystyrene/CO₂ system [69,84].

The CO₂-philic behavior of PMMA was compared with that of polystyrene by Reglero-Ruiz and colleagues [64]. After a saturation stage at 40 °C with a pressure of 30 MPa, they measured the CO₂ uptake of PMMA and PS samples (1.5 mm thick plaques). They showed that the gas uptake of PMMA was higher by more than 6 wt% compared with polystyrene.

Polymer/CO₂ affinity has to be taken into account in nano-foaming processes. Indeed, the foaming of CO₂-philic polymers allows us to obtain significant CO₂ uptakes with reduced saturation pressures and/or times. Moreover, CO₂ solubility within polymers may prove to affect cell nucleation and growth during the foaming stage.

3.2. Cell nucleation and growth

During the second stage of the foaming process, thermodynamic destabilization causes cell nucleation followed by cell growth. In the literature, the classical nucleation theory (CNT) is often used to explain the mechanisms of cell formation [85,86].

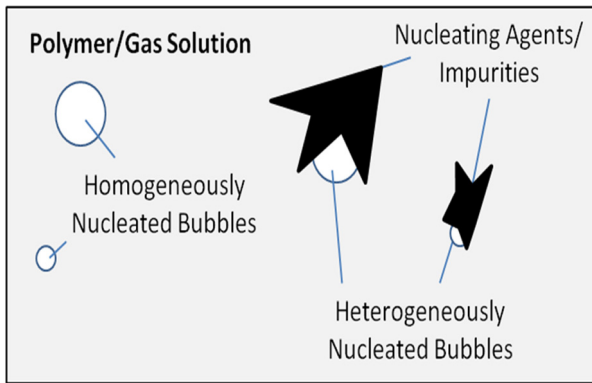


Fig. 10. Schema of homogeneous and heterogeneous nucleations in a polymer/gas system.

3.2.1. Cell nucleation theory

According to the classical nucleation theory, nucleation can appear in two distinct ways (see Fig. 10) that are called:

- homogeneous nucleation,
- heterogeneous nucleation, with nucleating agents.

In each case, this theory involves a cell critical radius r_{cr} : a cell whose radius is larger than the critical radius would spontaneously grow. Otherwise it tends to disappear.

3.2.1.1. Homogeneous nucleation. At room temperature, the polymer/gas system tends to minimize its free energy ΔG :

$$\Delta G = -\frac{4\pi r^3}{3} \Delta P + 4\pi r^2 \gamma \quad (19)$$

where r : cell radius; γ : surface tension; ΔP : level of supersaturation: pressure difference between the metastable solution and the nucleated phase of pure gas.

The free energy reaches a maximum value when $r=r_{cr}$. The system tends to reduce its free energy: cells whose radius is lower than r_{cr} resorb, whereas those whose radius is larger than r_{cr} grow [87]. When $r=r_{cr}$, the free energy derivative tends to zero, giving the following relation:

$$r_{cr} = \frac{2\gamma}{\Delta P} \quad (20)$$

Therefore, the nucleation appears when the energy barrier $\Delta G(r_{cr})$ is crossed:

$$\Delta G_{hom} = \frac{16\pi r^3}{\Delta P^2} \quad (21)$$

Thermodynamic destabilization during the nucleation stage provides additional energy to the polymer/gas system, decreasing the $\Delta G(r_{cr})$ and allowing cell formation. The rate of homogeneous nucleation can be estimated with the following relation:

$$N_{hom} = C_0 f_0 e^{-\Delta G/kT} \quad (22)$$

where C_0 : gas concentration; f_0 : frequency factor of gas molecules.

According to Eq. (22), a high CO_2 uptake by the polymer would lead to the formation of a large number of nucleation sites. It can also lead to the decrease of the average cell

size of the foam: Krause and colleagues [88] placed some poly(etherimide) (PEI) in a pressure vessel under different gas pressures and noticed, after foaming experiments, that an increase of 4 MPa causes a decrease in the cell size of more than one decade and a hundred-fold increase in the cell density. However, Costeux and colleagues [89] did not confirm this assumption for styrene acrylonitrile copolymer (SAN)/acrylic blends and showed that, for miscible blends, finer morphologies were obtained with higher SAN contents, corresponding to less CO_2 -philic blends. This shows that classical nucleation does not entirely explain nucleation mechanisms.

Moreover, it does not precisely take into account the influence of the pressure drop rate on final foam structures. In batch foaming processes, a high pressure drop rate between the saturation and the foaming stage tends to decrease the average cell size and increase cell density of produced foams by favoring nucleation rather than cell growth [90]. In this case, the gas desorption becomes lower during the pressure drop and prevents increasing of the energy barrier ΔG . Reglero-Ruiz and colleagues [91] showed that the increasing of the pressure drop rate from 1.2 to 15 MPa leads to the five decades increasing of the cell density of PMMA/acrylic copolymer foams. After a saturation stage at 30 MPa and 40 °C followed by a pressure drop rate of 15 MPa, they produced nano-cellular foam with cell density d_{cell} higher than 10^{14} cm^{-3} and a cell size of 300 nm.

However, during the pressure drop, the vessel temperature is also a key parameter that can reduce the effect of the pressure drop rate. Indeed, if the vessel temperature is rather low, the polymer viscosity can prevent cell growth [92]. This is what happens when the foaming process is carried out in two stages with a 'low temperature' saturation stage to maximize the CO_2 uptake. The pressure drop rate effect on the final foam morphology is low as the nucleation only appears when samples are transferred to a hot liquid bath. Mahmoodi and Behravesh [92] illustrated this phenomenon in the case of ABS sample foaming. In their process, the saturation stage, at room temperature with a gas pressure of 6 MPa, was followed by a pressure drop rate that varied from 0.005 to 6 MPa s^{-1} . The nucleation was then induced in a glycerin bath at 100 °C. The authors showed that similar foam morphologies were obtained after the nucleation stage, with average cell sizes around 2 μm and foam densities around 0.1 g cm^{-3} . According to them, the pressure drop step only causes gas supersaturation into polymer samples and is not significant enough to have an effect on cell nucleation.

3.2.1.2. Heterogeneous nucleation. The presence of fillers, impurities or spherulites in polymers is at the root of another nucleation phenomenon, called heterogeneous nucleation that appears in addition to homogeneous nucleation [93]. Indeed, in the presence of particles or irregularities, the free energy $\Delta G(r_{cr})$ decreases, and involves a reduction factor f such as [94,95]:

$$\Delta G_{het} = \Delta G_{hom} \frac{f(m,w)}{2} \quad (23)$$

$$m = \cos \theta = \frac{\gamma_{13} - \gamma_{23}}{\gamma_{12}} \quad \text{and} \quad w = \frac{R}{r_{cr}} (\text{relative curvature})$$

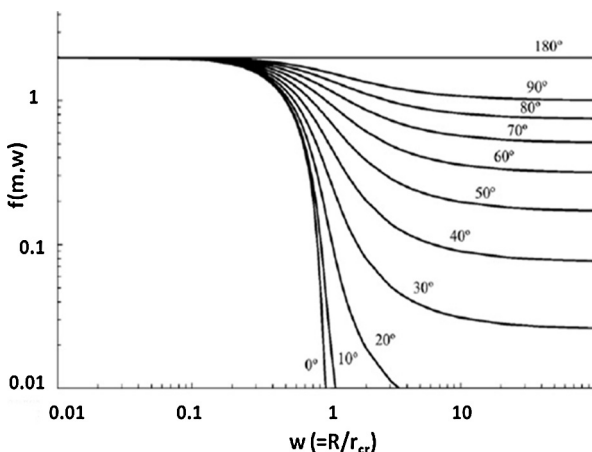


Fig. 11. Reduction factor f as a function of relative curvature and contact angle [95], Copyright 2010. Reproduced with permission from Elsevier Ltd.

where R : radius of the particles; γ_{13} , γ_{23} , γ_{12} : the polymer–nanoparticle, gas–nanoparticle, and polymer–gas interfacial tensions, respectively; θ : contact angle between the cell, polymer and particles.

The exact expression of $f(m,w)$ is given below:

$$f(m, w) = 1 + \left(\frac{1 - mw}{g} \right)^3 + W^3 \left[2 - 3 \left(\frac{w - m}{g} \right) + \left(\frac{w - m}{g} \right)^3 \right] + 3mw^2 \left(\frac{w - m}{g} - 1 \right) \quad (24)$$

with $g = (1 + w^2 - 2mw)^{0.5}$.

Fig. 11 represents the factor f as a function of the contact angle and of the relative curvature.

Qualitatively, a low contact angle and a large surface curvature lead to decrease the free energy $\Delta G(r_{cr})$ and consequently increase the rate of heterogeneous nucleation, equal to:

$$N_{het} = C_1 f_1 e^{-\Delta G_{het}/kT} \quad (25)$$

where C_1 : nucleating agents concentration; f_1 : frequency factor of gas molecules.

According to Eq. (25), the higher the nucleating agent concentration, the more the nucleation rate increases. Goren and colleagues [95] highlighted the effect of chemical nature and size of nucleating agents on the foaming of PMMA. They carried out foaming tests on PMMA/silica nanoparticle systems. Materials were first mixed with a Haake Benchtop extruder to obtain composites containing 1% silica by weight. Half of the nanoparticles were surface modified with fluorine containing a silane coupling agent (TFTOS). Five kinds of samples, with different particle sizes (see Table 4), were foamed with rapid pressure quenching after a saturation stage at 40 °C. Fig. 12 shows the cell density d_{cell} of each sample for various saturation pressures.

The presence of fillers causes an increase of cell density, compared with that of neat PMMA. We also note that the higher the particle size, the more the cell density increases. Moreover, an increase of the saturation pressure leads to the increase of the cell density. These results agree with the

Table 4
Notation for PMMA/silica nanocomposite samples [95].

Sample reference	Average particle size (nm)	Fluorinated particles
B150	150	/
F150	150	+
B15	15	/
F15	15	+

theory previously developed. Fluorinated coating on particles also causes increasing of the cell density. The authors put forward two assumptions to explain this result:

- the fluorinated coating allows a better dispersion of nanoparticles into the polymer matrix
- the latter can also decrease the global surface tension and the energy barrier $\Delta G(r_{cr})$.

3.2.1.3. Limitations of the classical nucleation theory. Even though the classical nucleation theory identifies the main parameters involved in the nucleation phenomenon, the assessment of the critical radius r_{cr} and the system free energy ΔG with this theory often differs from experimental results in the case of polymer/gas systems. For instance, it has been demonstrated that this theory predicts too high a level of supersaturation within polymer/nucleating agents/CO₂ systems. Wong and colleagues [96] highlighted the stress-induced nucleation effect in polymer/nanoclay systems: when a cell nucleates near a nanoclay particle, the local pressure P_{local} around the particles may be not equal to the system pressure. The polymer/gas system could be subject to local pressure variation ΔP_{local} and this has to be taken into account in the calculation of the critical radius and thus of the system free energy. In the presence of tensile stress, the critical radius would decrease and the supersaturation level would increase.

Kim and colleagues [97] compared classical nucleation theory with self-consistent field theory SFCT, in the case of nano-cellular foams. Unlike SFCT based on statistical mechanical calculations, the classical nucleation theory overestimates surface energies of nano-sized cells and hence the energy barrier for nucleation. Other theories, such as density-functional theory (DFT), have been developed to offset the shortcomings of the classical nucleation theory and show that the latter fails to capture the structural features of the cell nuclei [98,99].

3.2.2. Cell growth mechanisms

Once a nucleus is formed, its growth is generally described by continuum conservation equations. In the case of a polymer melt, if thermodynamic fluctuations allow nucleus growth, the latter is constrained by surface and viscous forces [100]. Shafi and colleagues [101] presented cell growth dynamics in a Newtonian fluid using the following equation:

$$\frac{dr}{dt} = \frac{r}{4\eta_{matrix}} \left(\Delta P - \frac{2\gamma}{r} \right) \quad (26)$$

where dr/dt : cell growth rate; η_{matrix} : viscosity of polymer matrix.

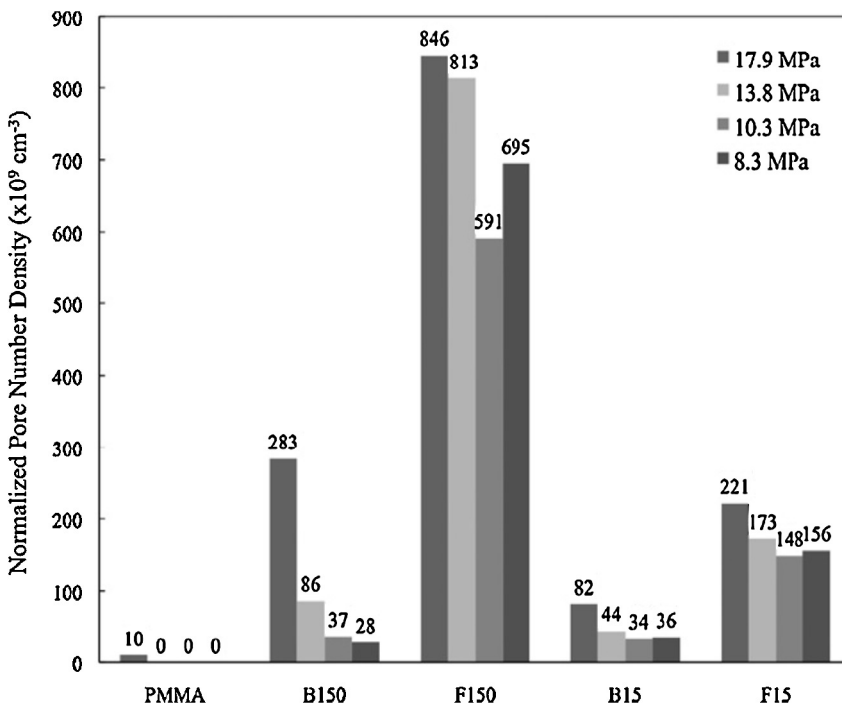


Fig. 12. Cell density d_{cell} of neat PMMA and PMMA/silica nanocomposites for various saturation pressures [95]. Copyright 2010. Reprinted with permission from Elsevier Ltd.

The viscosity η_{matrix} depends on both polymer molecular structure and content of dissolved CO₂ (as discussed in the following, the elongational viscosity may be more relevant than the shear viscosity) [102]. As the cell growth proceeds, the gas concentration at the cell surface decreases because of the decreasing pressure inside the cell. With time, a concentration gradient appears around cells and propagates in the polymer melt.

The viscosity of the polymer matrix/CO₂ system appears to be the first-order parameter to control the cell growth and to limit the coalescence phenomenon in foaming processes. However, Eq. (26) does not consider the viscoelastic behavior of polymer melts and the system has to be considered as a cell surrounded by a shell of viscoelastic fluid with a finite volume [87].

Although Eq. (26) can qualitatively predict the influence of process pressures and temperatures on the state of polymer/gas system (and thus on the cell growth), it does not depict the global role of the rheological behavior of polymers in the cell growth phenomenon. Moreover, two different CO₂ processes are often investigated: (1) a single-stage process in which nucleation is induced by a pressure drop quench after a saturation stage at 'high' temperature under supercritical conditions (a foaming process by extrusion, for example) and (2) a two-stage batch process with pressure or thermal quenching to induce cell nucleation and growth after a saturation stage at 'low' temperature under gaseous/supercritical conditions. As regards amorphous polymers, the viscoelastic behavior is quite different in these two processes.

In the case of the first process, the polymer is a viscoelastic liquid at these high temperatures far from the

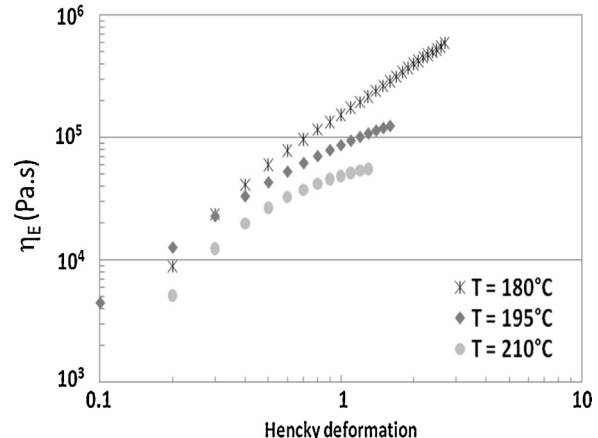


Fig. 13. Extensional viscosity as a function of time for uniaxial flow of neat PMMA ($M_w = 100,000 \text{ g mol}^{-1}$) at different temperatures at a constant extensional rate (10 s^{-1}).

T_g . For example, the variation in the extensional viscosity of a PMMA sample at $T = 210^\circ\text{C}$ is shown in Fig. 13. As, the cell growth process imposes high extensional action on the cell wall [103], the elongational viscosity has to be fitted to provide strain hardening in order to control the foam growth in micro- or nano-cellular foaming processes. Generally speaking, the use of branched polymers or long chain branches (LCB) is one of the research areas looking to stabilize cell growth and limit coalescence [104–106]. However, Otsuki and Kanai [107] showed, using a numerical simulation, that the strain-hardening characteristics of polymer does not strongly affect the cell growth rate,

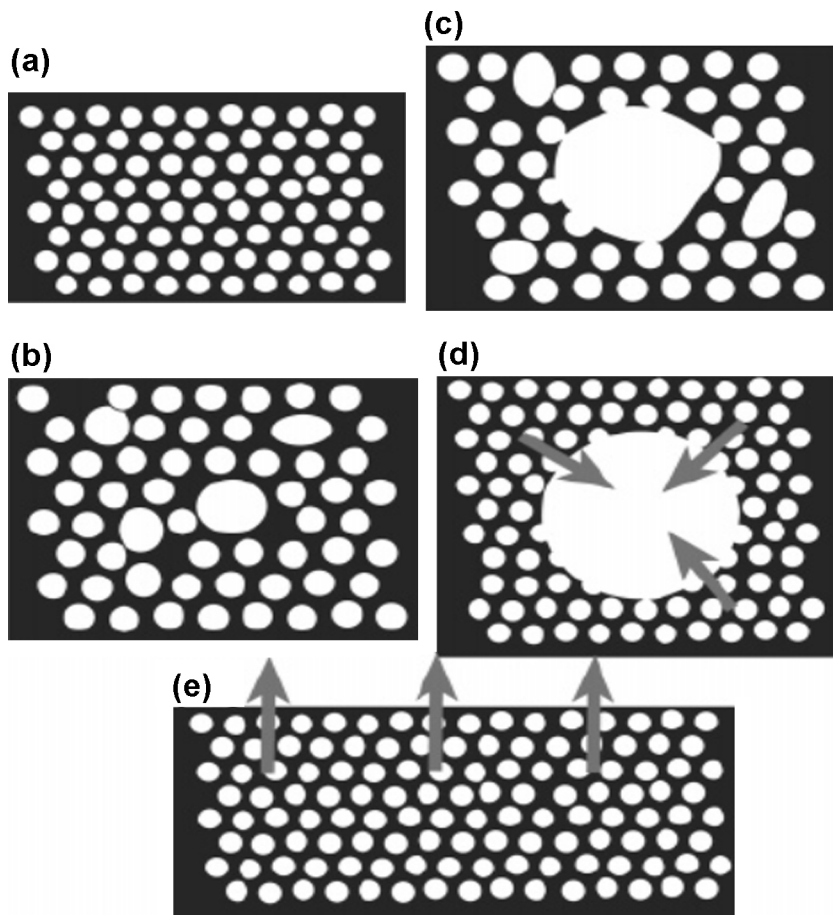


Fig. 14. Schematic illustration of cell formation at (a) $T_{nuc} \ll T_g$, (b) $T_{nuc} < T_g$, (c) $T_{nuc} = T_g$, (d) $T_{nuc} > T_g$ in polymer and (e) $T_{nuc} > T_g$ near surfaces [111]. Copyright 2005. Reproduced with permission from the American Chemical Society.

even for foaming processes at high temperature. The linear viscoelastic characteristic appeared to be more influential. This was confirmed by McCallum and colleagues [108], who worked on the effect of branched PP content on cell growth during foaming of thermoplastic olefins in a batch foaming process at high temperature (180°C). The authors showed that strain hardening of blends did not influence the cell growth rate. Indeed, the most relevant rheological parameter for the growth rate process was the high frequency elastic modulus data, similar for all PP blends.

In batch CO_2 foaming process with saturation stage at 'low temperature', the polymer/ CO_2 system can be considered as viscoelastic solid near the T_g (rubbery behavior when the temperature is just higher than the T_g). At these temperatures, strain-hardening is obviously the rheological behavior as the polymer is deformed in the rubbery zone. Consequently, the stress is directly proportional to the deformation, as shown in Fig. 13 (extensional viscosity at $T=180^\circ\text{C}$).

A few studies focus on the role of polymer rheology on the final foam structures fabricated in such processes. Liao and colleagues [109] investigated the foaming of long-chain branching PSSs (polystyrenes). Rheological measurements showed that LCB PSSs exhibit strain-hardening behavior compared with neat PS samples. Foaming

experiments (at 80°C) showed that the cell density increases, but only micro-foams are produced. To explain these results, the authors suggested that the cell growth dynamics of the branched samples would be hindered during the foaming process compared with the linear ones because of their increased elongational viscosity. Stafford and colleagues [110] worked on the foaming of polystyrene samples with different molecular weights. They found that variations in molecular weight and polydispersity of polymers did not have any significant influence on final foam structures. This could reflect that the influence of the rheological behavior of polymers on the control of the foaming is complex and not yet well understood.

In batch foaming processes, the cell growth also depends on the foaming stage temperature. Indeed, according to the classical nucleation theory, the decreasing of foaming temperature T_{nuc} leads to the formation of smaller cells whose growth is restricted by an excessively high matrix viscosity. However, opinions differ in the literature as to the lowest temperature for which foaming is possible. Yokoyama and Sugiyama [111] proposed the illustration in Fig. 14.

When T_{nuc} is below the polymer/gas T_g , nano-cells appear because of the high viscosity of the polymer matrix. However, if the temperature is too far below T_g , a high

pressure drop rate can cause polymer cracking. Micro-cells appear when the foaming temperature is near the polymer/gas T_g . When $T_{nuc} > T_g$, the gas uptake decreases because of the high gas diffusion, releasing the residual pressure within cells and limiting the growth of nano-cells. Krause and colleagues [88] affirm that cell nucleation does not appear below the polymer/gas T_g and limits the necessary conditions for obtaining cellular materials to a temperature range between the polymer/gas T_g and a maximum temperature T_{max} higher than this T_g . When $T_{nuc} > T_{max}$, the foam density no longer depends on the CO₂ uptake. When the temperature tends to the polymer/gas T_g , cell density is maximum. In another study, Krause and colleagues [112] also reduced this temperature range and affirmed that the foaming temperature has to be higher than the polymer/gas T_g and lower than the glass transition of the neat polymer.

3.2.3. Conclusion

We have shown that many parameters are involved in polymer foaming, such as process parameters or initial sample microstructure. According to previously described theories, key mechanisms of cell nucleation, CO₂ swelling and necessary foaming conditions have to be controlled to produce nano-cellular foams, with high cell density and low cell size, in batch foaming processes.

On the one hand, the preferred nucleation rate provides both high thermodynamic instability (high temperature and pressure gradients) and significant CO₂ uptake. On the other hand, the cell growth has to be limited to prevent micro-foam formation. Therefore, the thermodynamic instability has to be low, that goes against previously stated requirements. Consequently, compromises have to be made, especially regarding temperature and pressure variations, to increase the nucleation rate while limiting the cell growth. Moreover, the cell growth and coalescence phenomena have to be limited by the surrounding polymer/gas matrix, but the influence of the polymer/gas matrix viscosity is not obvious at the nano-scale in batch foaming processes.

However, we have already shown that obtaining nano-cellular foams using a batch CO₂ foaming process is possible with specific polymers such as PEI [25,26]. Moreover, the BASF Company has also published a patent on the nano-foaming of *more classical* neat polymers [113]: in a batch foaming process under supercritical conditions with very high pressure drop rates ($\approx 40 \text{ GPa s}^{-1}$), low density nano-cellular foams of PMMA were obtained, with average cell sizes between 40 and 150 nm and foam densities between 0.15 and 0.3 g cm⁻³.

Nevertheless, in most cases and under less severe conditions, the foaming of neat polymers does not result in nano-cellular foams even with optimized foaming batch processes [91,95,114]. Micro-cells are often produced with cell density lower than 10¹¹ cm⁻³.

4. Fabrication of nano-cellular polymers from nanostructured materials

In the attempt to reach much higher cell densities and control cell growth, the foaming of nano-structured

polymer or copolymers materials has been developed to take advantage of heterogeneous nucleation or to limit the cell growth within CO₂-philic nano-domains dispersed in a 'rigid' matrix (selective foaming). The final part of this review focuses on the latest developments of these techniques to obtain nano-cellular foams.

4.1. Foaming of neat block copolymers

The foaming of nano-structured polymer materials would allow higher nucleation rates than the foaming of neat polymers by causing heterogeneous nucleation. Moreover, in some cases, the material nano-structuration would prevent the formation of micro-cells. Indeed, one way to gain better control of the cell formation is to limit the foaming to a dispersed phase more CO₂-philic than the surrounding polymer matrix. Section 3.1.3 refers to some CO₂-philic polymers such as fluoro- or acrylate polymers that can be used by this way. Yokoyama and Sugiyama [111] give an example of the foaming of a block copolymer composed of nano-domains of more CO₂-philic phase. During the foaming process, gas expansion causes cell nucleation inside CO₂-philic domains. Internal pressure expands the cells and causes copolymer chains to stretch in the peripheral direction and their compression in the radial direction. Elastic forces become sufficiently significant to limit the cell growth.

The obtaining of nano-cellular foams would require an initial nano-structured material with a CO₂-philic nodule size lower than 100 nanometers to take advantage of the Knudsen effect after the foaming process. The nodule density must also be close to the final required cell density (near 10¹⁵ cm⁻³ according to Section 2.3) to reduce the final solid matrix content and thus limit the solid phase contribution to the thermal conductivity. Moreover, the viscosity of the matrix has to limit the cell growth during the foaming process. To that end, the matrix/gas system must have a higher viscosity than that of nodules/gas system.

Applying this principle, Taki and colleagues [115] obtained nano-cellular foams of PS-b-PMMA copolymer. The latter was first dissolved in toluene then coated on a silicon wafer. The film was dried at room temperature for several hours and then annealed in vacuum at 170 °C to cause nano-structuration. After foaming under supercritical conditions, foam with an average cell size of 40 nm was obtained, as shown in Fig. 15. However, although the film density is not disclosed in the study, Fig. 15 shows that the solid phase predominates: the thickness of inter-cell walls is the approximate size of cells.

Many studies [116–118] focus on the foaming of fluoro-copolymers such as PS-PFMA (poly(perfluorooctylethyl methacrylate)) block copolymer. Indeed the fluorinated block is considered as more CO₂-philic than the polystyrene block. Investigated saturation pressures were near 30 MPa. Yokoyama and Sugiyama [111] carried out foaming tests on PS-PFMA copolymer films. The obtained cell densities d_o are higher than 10¹⁵ cm⁻³ with average cell sizes lower 50 nm (see Fig. 16). The authors highlight the CO₂-philic behavior of PFMA block, in that nucleation and cell growth appear during the foaming process.

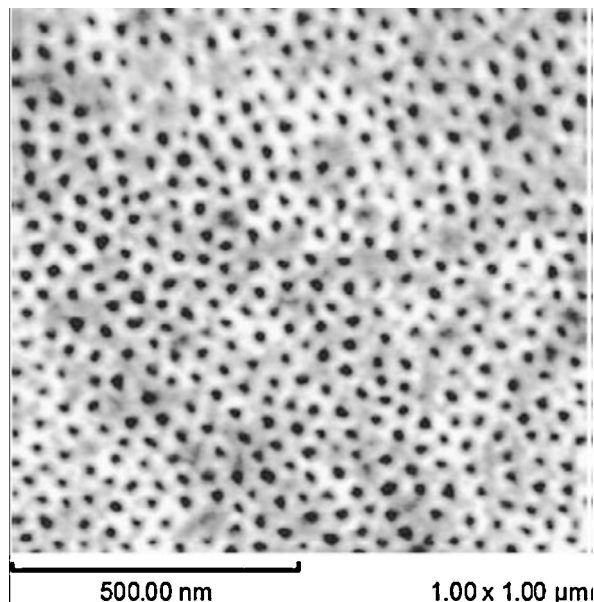


Fig. 15. SEM image of PS-b-PMMA copolymer thin film after foaming process ($20^{\circ}\text{C}/8.6\text{ MPa}$, pressure drop rate 0.5 MPa min^{-1}) [115]. Copyright 2008. Reproduced with permission from WILEY-VCH Verlag GmbH & Co. KGaA, Weinheim.

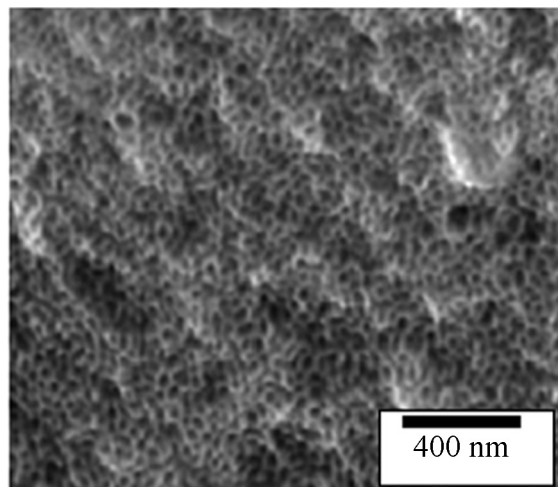


Fig. 16. SEM image of PS-PFMA copolymer film after foaming process ($30^{\circ}\text{C}/60\text{ MPa}$, pressure drop rate 0.5 MPa min^{-1} at $T=0^{\circ}\text{C}$) [111]. Copyright 2005. Reproduced with permission from the American Chemical Society.

The foaming of films of PMMA-PFMA block copolymers has also been investigated with similar sample preparation and foaming conditions in another study [63]. Even if PMMA block can be considered as CO_2 -philic, its glassy state during the foaming process would prevent the collapse of the swollen cells of the fluorinated block. Foam porosities appeared to be lower than 30% but nano-cells between 20 and 70 nm were obtained.

Reglero-Ruiz and colleagues [119] worked on the foaming of films of PS-PFDA (1,1,2,2-dihydroperfluorodecylacrylate) block copolymer, synthesized by ATRP, with

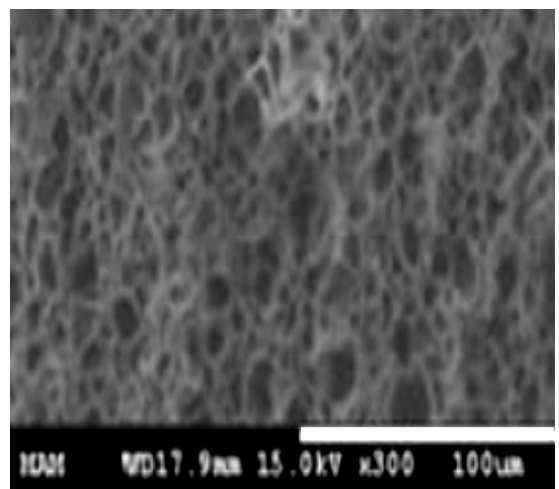


Fig. 17. SEM image of MAM copolymer plaque after foaming process ($40^{\circ}\text{C}/30\text{ MPa}$, pressure drop rate 15 MPa min^{-1}) [16]. Copyright 2010. Reproduced with permission from the Society of the Chemical Industry.

saturation stage under supercritical conditions (30 MPa , 0°C). They showed that the presence of the fluorinated block increases the CO_2 uptake from 9 wt% to 32 wt% (compared with neat PS film). Moreover, after the depressurization, they obtained nano-cellular materials with cells of about 100 nm and cell density d_0 of $7.3 \times 10^{14}\text{ cm}^{-3}$, whereas no cellular structure appeared in the foaming experiment on PS film. According to the authors, as in previously cited studies, cell growth occurs in the fluorinated blocks but is restricted by the surrounding rigid PS matrix.

However, in most cases, block copolymer synthesis and foaming processes remain complex and involve several stages. Moreover, foaming experiments on copolymers were carried out on films and do not reflect the sorption and desorption phenomena that appear in bulk polymer materials. Nucleation and cell growth mechanisms could also be affected by the anisotropic characteristic of such materials. These considerations make such a foaming process difficult to develop on the industrial scale.

Other studies focus on the foaming of bulk commercialized copolymers, such as MAM poly(methyl methacrylate-b-butyl acrylate-b-methyl methacrylate) block copolymer-

Reglero-Ruiz and colleagues [16] studied the foaming of Altuglas MAM copolymer (30/40/30 wt%). According to these authors, MAM copolymers have very high affinity with CO_2 , that could increase, in a nanostructured assembly, the nucleation rate. More precisely, in another study [91], the authors considered MAM material as a copolymer with a highly CO_2 -philic and rubbery block, where foaming preferentially occurred, and a less CO_2 -philic rigid block. They injected 3 mm thick plaques and foamed them under supercritical conditions. Obtained foam densities varied from 0.1 to 0.2 g cm^{-3} with cell size greater than $10\text{ }\mu\text{m}$ (see Fig. 17). Foam densities, cell sizes and thermal conductivities of MAM copolymer foams are reported in the following table.

According to Table 5, the higher the cell size, the greater the foam density and the thermal conductivity decrease.

Table 5

Values of foam density, cell size and thermal conductivity of MAM copolymer foams [16].

Pressure drop time (min)	Foam density (g cm^{-3})	Cell size (μm)	Thermal conductivity ($\text{W m}^{-1} \text{K}^{-1}$)
2	0.20	9	0.0628
8	0.18	44	0.0627
10	0.16	51	0.0589
15	0.15	61	0.0599
30	0.14	98	0.0556

In contrast to previously reported studies, foam densities are low, but average cell sizes remain too high to lead to a reduction of the thermal conductivity by the Knudsen effect. According to the authors, these results derive from the low rigid phase content of the MAM copolymer that was not significant enough to restrain the cell growth.

4.2. Foaming of polymers nanostructured with nano-fillers

The blending of polymers with nano-fillers is another way to obtain finer foam microstructures. Indeed, the blend nano-structuration, caused by the presence of dispersed nano-fillers, induces heterogeneous nucleation within material. Some studies [103,120] refer to the effect of carbon nanotubes or graphite on nucleation rates within polymer/nano-filler systems in batch foaming processes. However, although heterogeneous nucleation allowed the increase of cell densities, only micro-cells were produced with cell densities d_o lower than $10^{11} \text{ g cm}^{-3}$.

The use of modified clays has also been investigated. Ito and colleagues [121] worked on the foaming of pelletized extruded strands of polycarbonate (PC)/fluorohectorite (organically modified clay) blends, using a foaming process with a saturation stage under supercritical conditions followed by a foaming stage in a silicone oil bath. However, the presence of clays (with contents lower than 5 wt% in blends) does not significantly increase the cell density compared with unfilled polymer and the cell size remains higher than $1 \mu\text{m}$.

Layered double hydroxides (LDH), considered as synthetic inorganic/organic anionic clays, have been investigated by Martinez and colleagues [122] as nucleating agents in PMMA and PS matrices. Foaming experiments were carried out on 1.5 mm thick plaques. After a foaming process with a saturation stage under supercritical conditions and a foaming stage in a silicone oil bath, foams of PS/LDH and PMMA/LDH systems were produced with cell sizes of about $2 \mu\text{m}$ and cell densities d_o higher than 10^{10} cm^{-3} . This corresponds to a cell density increase of about three decades compared with neat polymer foam in the case of PS/LDH foam, whereas for PMMA/LDH foam, the cell density increase was less than one decade. The influence of the nucleating agents appears in both cases, but is lower in the case of PMMA/LDH systems. Indeed, because of the great affinity of PMMA with SiO_2 , the effectiveness of nucleating agents appears to be lower than in PS-based systems because of the initial difference between PS and PMMA matrix in terms of homogeneous nucleation.

Table 6

Cellular structure characterization results- PMMA/oMMT foams [123].

	Foam density (g cm^{-3})	Cell size (μm)	Cell density d_o (cm^{-3})
PMMA	0.824	8.1 ± 1.5	3.6×10^9
PMMA/2.5 wt%	0.630	0.50 ± 0.03	9.2×10^{12}
oMMT			
PMMA/5 wt%	0.633	0.46 ± 0.01	1.4×10^{13}
oMMT			
PMMA/10 wt%	0.597	0.29 ± 0.01	3.2×10^{13}
oMMT			

In another study [123], the authors produced nano-cellular foams of PMMA/organically modified montmorillonite (oMMT) blends, using a similar foaming process. Obtained average cell sizes, foam and cell densities are summarized in Table 6 according to oMMT content.

Note that the increase of the oMMT content to 10 wt% in blends leads to an increase of the cell density d_o (up to four decades compared with PMMA foam). This cell density increase causes a decrease of the foam density from about 0.8 to 0.6 g cm^{-3} . Moreover, cell size becomes less than $0.5 \mu\text{m}$ for all PMMA/oMMT foams.

Siripurapu and colleagues [124] investigated the foaming of films of PMMA/Nano-silica particles (until 12 wt%) blends with a batch foaming process under supercritical conditions. They highlighted the influence of nano-silica particles presence on cell nucleation at high temperature (higher than 80°C) and showed that particles stabilize cell nuclei, resulting in higher cell densities. However, only micro-cells were produced with cell densities d_o lower than 10^{12} cm^{-3} .

Zhai and colleagues [125] also used nano-silica particles as nucleating agents within polycarbonate (PC) matrix, investigating the foaming of 1 mm thick plaques. They showed that the blending of polycarbonate (PC) with 9 wt% of silica nanoparticles can increase the cell density d_o from 2×10^{11} to $6 \times 10^{12} \text{ cm}^{-3}$ and reduce the cell size distribution during the foaming process (see Fig. 18). The average cell size decreases from about $1.4 \mu\text{m}$ to $0.4 \mu\text{m}$.

Costeux and Zhu [24] obtained finer foam structures by adding lower nano-silica particle content (3 wt%) to a PMMA matrix. They investigated the foaming of 3 mm thick plaques, using a saturation stage at 30 MPa and 60°C followed by a high pressure drop rate. The blending of PMMA with SiO_2 decreased the average cell size from 0.9 to $0.28 \mu\text{m}$ with increasing cell density d_o from 10^{11} to $3 \times 10^{14} \text{ cm}^{-3}$. The addition of an annealing stage in a water bath at 80°C decreased the average cell size to 140 nm and increased the cell density d_o to $2.4 \times 10^{15} \text{ cm}^{-3}$ (see Fig. 19). Note that these values approach those previously presented in Section 2.3.

4.3. Foaming of polymers nanostructured with block copolymers

Sections 3.2 and 4.2 refer to the heterogeneous nucleation phenomenon in polymer/inorganic filler blends, that leads to the obtaining of more homogeneous and finer cellular structures. However, heterogeneous nucleation also appears in organic multiphase systems produced from

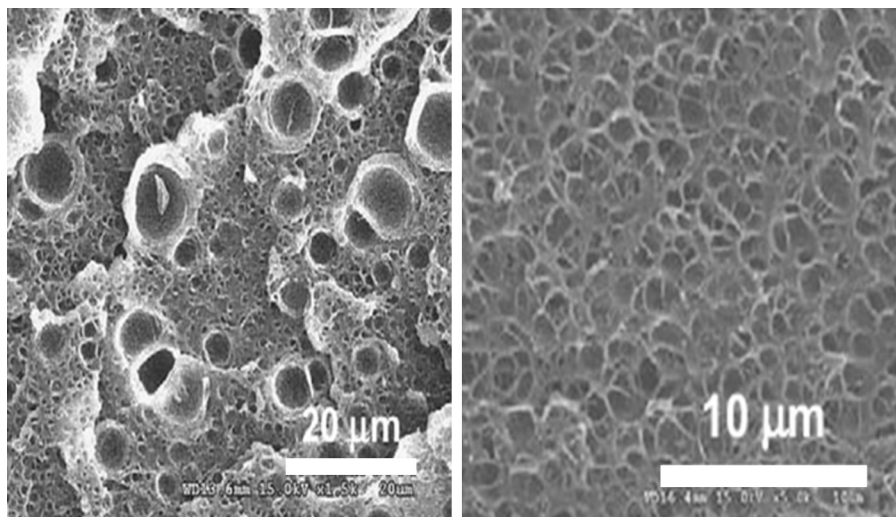


Fig. 18. SEM images of (left) neat PC and (right) PC + 9 wt% silica (50 °C/20 MPa, foaming stage at 120 °C) [125]. Copyright 2006. Reproduced with permission from Elsevier Ltd.

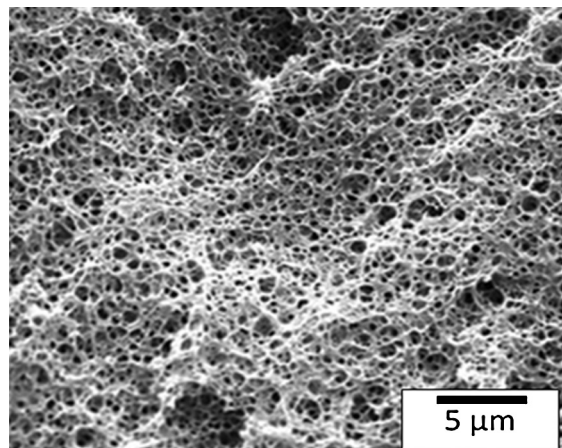


Fig. 19. SEM image of PMMA/nano-silica particles (3 wt%) foam (40 °C/30 MPa, high pressure drop rate, annealing in a water bath at 80 °C) [24]. Copyright 2013. Reproduced with permission from Elsevier Ltd.

polymeric material blends such as polymer/copolymer copolymer/copolymer blends.

Some studies refer to the foaming of ABS terpolymers. The latter consist of an acrylonitrile-styrene copolymer (AS) matrix in which rubber particles (cross-linked butadiene grafted with AS copolymer) are dispersed [126]. Although ABS terpolymers are not considered as CO₂-philic materials, their specific morphologies can improve the nucleation rate during the foaming process. Indeed, interfaces between rigid and soft phases and their difference in terms of *T_g* can cause heterogeneous nucleation in addition to homogeneous nucleation [127]. Nawaby and colleagues [53] worked on the foaming of 0.65 mm thick sheets of ABS, previously compressed at 210 °C. The foaming process was carried out with a saturation stage at 0 °C and 3.4 MPa and a nucleation stage in a hot glycerin bath. In this study, the foaming process is optimized by making

use of the retrograde vitrification behavior of ABS. Several nucleation temperatures were investigated (see Fig. 20). These experiments show that the nucleation temperature increase causes a decrease in the foam density. Indeed, a high temperature improves cell growth, because of the decrease in the matrix viscosity.

The lowest-density foam (0.15 g cm⁻³) had a cell density *d_o* of about 3×10^{12} cm⁻³ with an average cell size lower than 1 μm. Nanometric cell sizes were not obtained, but the cell size decreased by more than one decade compared with the *iso*-density MAM foams in Reglero-Ruiz and colleagues' study [16]. This foaming batch process was carried out in another study by Murray and colleagues [128], for 1.5 mm thick plaques of ABS. The saturation pressure was 5 MPa at 27 °C and the nucleation stage was carried out in a glycerin bath at 80 °C. The foam had a cell density *d_o* of 1.4×10^{13} cm⁻³ with an average cell size of 0.54 ± 0.27 μm. Although the obtained cell size was more than 0.5 μm, low-density foams were produced. Moreover, such foaming processes provide nano-cellular foams, without requiring high saturation pressures during the saturation stage.

Nemoto and colleagues [129] carried out foaming experiments on 200 μm sheets of polypropylene/HSIS (hydrogenated styrene-isoprene-styrene copolymer) blends (80/20 wt%). Samples (as 200 μm thick sheets) were foamed in an ethylene glycol bath after a saturation stage in supercritical conditions. During the foaming process, elastomeric domains of isoprene were above their *T_g*, unlike the thermoplastic matrix, limiting the cell growth within the restricted dispersed phase. SEM analysis of foamed samples showed that cells were produced from 200 to 400 nm (see Fig. 21). However, the highest cell density *d_{cell}*, 7×10^{13} cm⁻³, was not high enough to obtain low-density nano-foams and foam densities were higher than 0.5 g cm⁻³.

The use of spherical block copolymer micelles as nucleating agent in the formation of microcellular foams has been investigated by Spitaël and colleagues [130]. Using

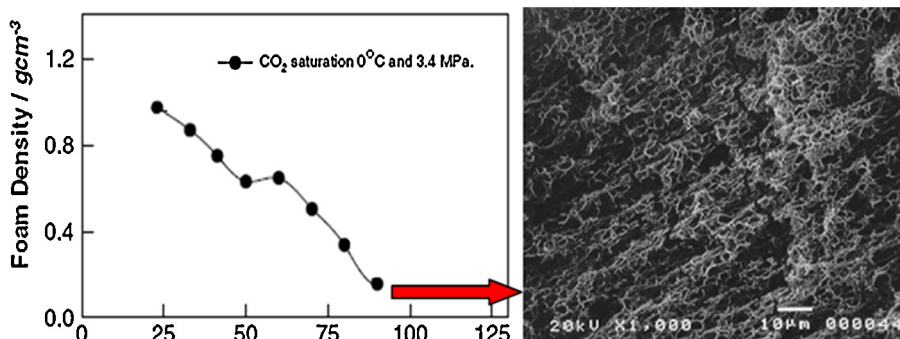


Fig. 20. Foam density as a function of foaming temperature – SEM image of ABS copolymer foam (density 0.15 g cm^{-3}) [53]. Copyright 2006. Reproduced with permission from the Society of the Chemical Industry.

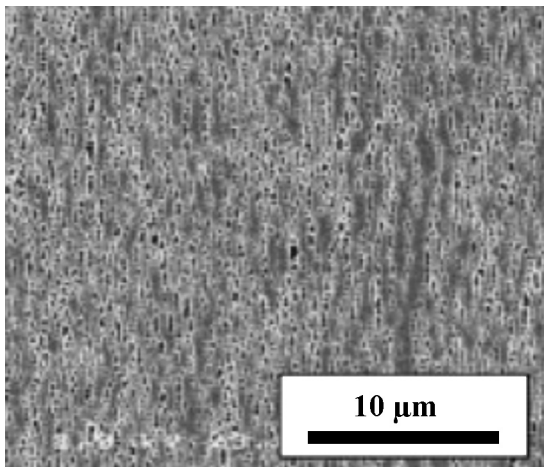


Fig. 21. SEM image of foamed PP/HSIS (20 wt%) ($25^\circ\text{C}/20 \text{ MPa}$, pressure drop rate 0.1 MPa min^{-1}) [129]. Copyright 2008. Reproduced with permission from WILEY-VCH Verlag GmbH & Co. KGaA, Weinheim.

low contents (<2 wt%) of PS-b-PMMA and PS-d-PDMS (poly(dimethylsiloxane)) di-block copolymers added to a polystyrene matrix, they studied the nucleation behavior of the resulting blends in a batch foaming process at low pressure (with gaseous CO_2). However, no significant increase of the cell density was observed (with values around 10^{10} cm^{-3}). This could in part be because of the resulting low CO_2 uptake of such polystyrene-based materials (about 7 wt%). Moreover, according to the authors, the size of micelle, less than 40 nm, may be smaller than the minimum effective size and thus decrease the nucleating agent effectiveness.

Reglero-Ruiz and colleagues [131–133] worked on the foaming of PMMA/MAM copolymer blends. The authors [16] had already shown that the foaming of MAM copolymers led to low-density foams with micro-cells, whose growth was not restrained. However, MAM copolymers can also act as nucleating agents in a polymer/copolymer blend. In particular, Reglero-Ruiz and colleagues studied the foaming of PMMA/MAM blends with a MAM content of 10 wt% (90/10 wt%) [134]. A MAM copolymer is composed of 70 wt% of methyl methacrylate. PMMA/MAM blends were injected to obtain 3 mm thick plaques. The foaming

process was the same as for the foaming of MAM copolymers, with a saturation stage at 30 MPa and 20°C , followed by a pressure drop rate of 15 MPa min^{-1} . The final foam structure is compared with that of neat PMMA foam in Fig. 22.

In the case of PMMA foam, the cell size is more than $5 \mu\text{m}$, whereas the cell size of PMMA/MAM foam is about 200 nm. Moreover, the cell density d_{cell} increases from 1.6×10^{10} to $4.5 \times 10^{14} \text{ cm}^{-3}$. These values approach those previously presented in Section 2.3. Foam density also decreases from 0.7 to 0.4 g cm^{-3} . These data gave a d_0 value at $1 \times 10^{15} \text{ cm}^{-3}$ in the case of PMMA/MAM foam. According to the authors, these differences are because of the CO_2 -philic behavior of the MAM copolymer, that improves the global CO_2 uptake (see Table 7). Moreover, the copolymer dispersion in the PMMA matrix also causes increase of the nucleation rate by heterogeneous nucleation.

Costeux and Zhu [24] carried out foaming tests on SAN (styrene/acrylonitrile) copolymer plaques 3 mm thick, with a saturation stage at 33 MPa and 30°C followed by a high pressure drop rate. Samples were then removed from the autoclave and annealed in a water bath at 60°C to complete foaming. The obtained foams had an average cell size of $2 \mu\text{m}$. The blending of SAN copolymer with POSS (0.25 wt%), a methacryl-substituted polyhedral oligomeric silsesquioxane (Sigma-Aldrich), decreased the average cell size to $0.2 \mu\text{m}$ with an increase of cell density d_0 from 4.5×10^{11} to $5.5 \times 10^{14} \text{ cm}^{-3}$.

The authors also worked on the foaming of P(MMA-co-EMA) copolymer (random copolymer of MMA with 50 wt% ethyl methacrylate)/POSS blends with 0.25 wt% POSS. According to the authors, P(MMA-co-EMA) is a highly CO_2 -philic copolymer, compared with the SAN copolymer. With this system, they obtained nano-foams with a cell size of 65 nm, a cell density d_0 of $2 \times 10^{16} \text{ cm}^{-3}$ and a porosity of 74% (equivalent to a foam density around 0.3 g cm^{-3}) (see Fig. 23).

Table 7
 CO_2 uptake after a 16-hour saturation stage under pressure of 300 bar [134].

Materials	CO_2 uptake (wt%)
PMMA	18.1
PMMA/MAM blend	25.6

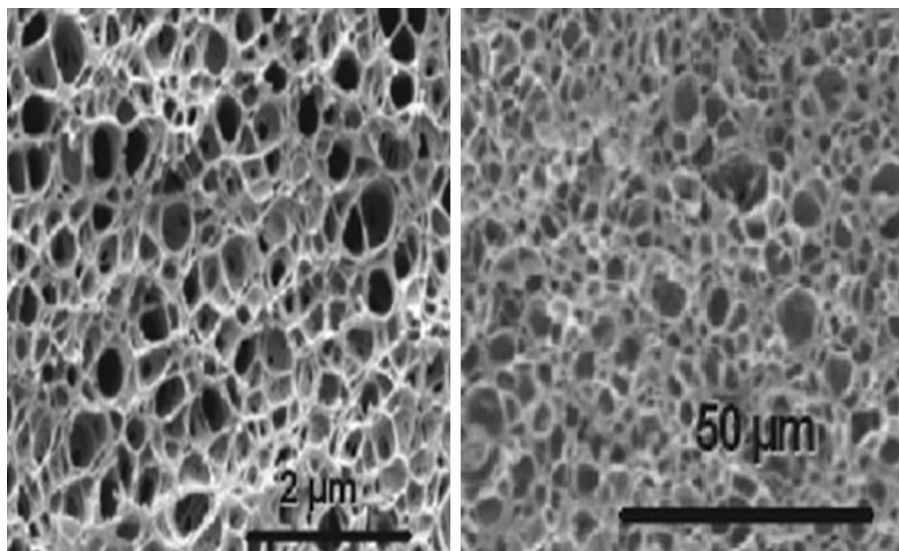


Fig. 22. SEM images of (left) PMMA/MAM (90/10 wt%) foam and (right) PMMA foam after foaming process (20 °C/30 MPa, pressure drop rate 15 MPa min⁻¹) [134]. Copyright 2011. Reproduced with permission from WILEY-VCH Verlag GmbH & Co. KGaA, Weinheim.

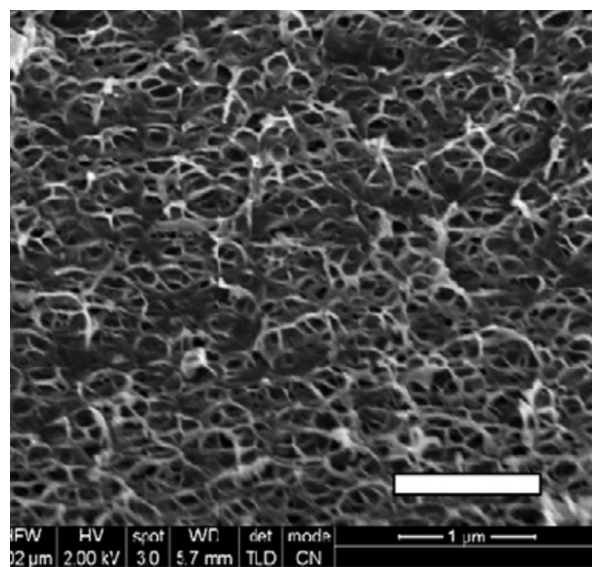


Fig. 23. SEM image of P(MMA-co-EMA)/POSS (0.25 wt%) foam after CO₂ foaming (35 °C, 33 MPa, high pressure drop rate, annealing in a water bath at 55 °C) [24]. Copyright 2013. Reproduced with permission from Elsevier Ltd.

This reveals that POSS acts as nucleating agents to facilitate the formation of nano-foams, even at very low concentration. Indeed, in the same study, the authors investigated the foaming of a PMMA/SiO₂ particle system with 3 wt% of fillers, as reported in Section 4.2. Although the foaming conditions and polymer matrix differ, the use of SiO₂ fillers as nucleating agents in PMMA allows the obtaining of nano-structures similar to SAN/POSS foams but with much higher content of potential nucleating agents. This puts emphasis on the efficiency of the different potential nucleating agents. Moreover, to explain this phenomenon, the authors first highlight the classical

heterogeneous nucleation phenomenon, but also suggest another nucleation mechanism: indeed, no measurable difference in melt viscosity, CO₂ solubility and *T_g* were detected, and SAXS experiments did not reveal aggregation. Yet POSS molecules could contribute to the formation of nuclei if the polymer/POSS interface shows enrichment in CO₂, or if POSS molecules act as an interfacial agent at the CO₂/bulk interface of expanding nuclei. Both effects could reduce the nucleation barrier. Investigations are still in progress to gain insight into these mechanisms.

In another study, using a similar foaming process, Costeux and colleagues [89] investigated the foaming of SAN/P(MMA-co-EMA) copolymers and SAN/PEMA (poly(ethyl methacrylate)) copolymer blends. In both cases, nano-cells were produced with a cell size of about 90 nm and cell densities *d₀* between 1 and 5 × 10¹⁵ cm⁻³, corresponding to porosities of about 60%. Moreover, as reported in Section 2.2.1, the authors showed that the use of a less CO₂-philic blend can produce finer cell structures without loss of porosity. They suggested that phase separation could occur under high pressure for miscible blends and cause CO₂ concentration fluctuations, promoting very high cell density as the system was subsequently foamed by high pressure drop. This shows that nucleation mechanisms in nanostructured-polymer materials appear to be complex and have not been fully explained; they depend on many parameters, such as local gas concentration and phase interfaces at the nano-scale.

4.4. Conclusion

In the studies cited in the preceding, the control of the nucleation rate and cell growth during the foaming process is improved by selective foaming or preferably heterogeneous nucleation within nanostructured polymer materials. Studies focusing on block copolymer foaming (see Table 8a) have shown that nano-cells less than

Table 8

Summary of the nano-foams obtained from copolymers or nanostructured blends. Study data – calculated values.

	Authors	Materials	Average cell size (nm)	Cell density d_o/d_{cell} (cm^{-3})	Foam density (g cm^{-3})	Thermal conductivity ($\text{W m}^{-1} \text{K}^{-1}$)
(a)	Sundaram and Li [25]	PEI	240	–	0.29	0.018
			86	–	0.26	0.013
	Taki et al. [115]	PS-PMMA block copolymer	40	–	–	–
	Yokoyama and Sugiyama [111]	PS-PFMA block copolymer	<50	4×10^{15} –	–	–
	Dutriez et al. [63]	PMMA/PFMA block copolymer	<70	–	>0.7	–
	Reglero Ruiz et al. [119]	PS-PFDA block copolymer	100	7.3×10^{14} –	>0.7	–
(b)			9000	9.3×10^9 –	0.2	0.0628
			98,000	1.4×10^7 –	0.14	0.0556
	Reglero-Ruiz et al. [16]	MAM block copolymer				
	Realinho et al. [123]	PMMA/oMMT blend	500	9.2×10^{12} –	0.63	–
			460	1.4×10^{13} –	0.63	–
			290	3.2×10^{13} –	0.60	–
	Zhai et al. [125]	PC/SiO ₂ blend	400	6×10^{12} –	–	–
	Costeux and Zhu [24]	PMMA/SiO ₂ blend	280	3×10^{14} –	0.22	–
	Nemoto et al. [129]	PP/HSIS blend	140	2.4×10^{15} –	0.26	–
	Nawaby et al. [53]	ABS terpolymer	200–400	$\sim 7 \times 10^{13}$	>0.5	–
(c)	Murray et al. [128]	ABS terpolymer	470	3×10^{12} –	0.15	–
	Reglero-Ruiz et al. [131–134]	PMMA/MAM blend	540	1.4×10^{13} –	0.38	–
			200	1×10^{15} 4.5×10^{14}	0.4	–
	Costeux and Zhu [24]	SAN copolymer/POSS blend	200	5.5×10^{14} –	0.32	–
			65	2×10^{16} –	0.30	–
		P(MMA-co-EMA)/POSS blend	99	1×10^{16} –	0.18	–
	Costeux et al. [89]	SAN/P(MMA-co-EMA) blend	99	3.1×10^{15} –	≈ 0.6	–
			91	4.9×10^{15} –	≈ 0.6	–
			86	4.5×10^{15} –	≈ 0.6	–
		SAN/PEMA blend	96	3.1×10^{15} –	≈ 0.6	–
			95	3.4×10^{15} –	≈ 0.6	–

100 nm in size could be produced with batch foaming processes. However, although few data are given concerning foam densities, microscopic images often reveal that this technique does not allow the fabrication of low-density nano-cellular materials. On the other hand, the nano-structuration of polymer materials with fillers or copolymers to increase the global nucleation rate during the foaming process appears to be an interesting way to obtain nano-cellular foams with cell densities higher than 10^{13} cm^{-3} (see Table 8b). In most cases, the obtaining of nano-cellular foams with a cell size less than 100 nm seems to be difficult. Moreover, although this technique improves the nucleation rate compared with the foaming of neat polymers, densities of nano-cellular foams are generally higher than 0.3 g cm^{-3} , because of the decrease of the cell size combined with an increase of the nucleation rate that is not significant enough to obtain very low density materials. Nevertheless, in specific cases, foams with cell size less than 100 nm and density between 0.1 and 0.2 g cm^{-3} were produced, combining high homogeneous and heterogeneous nucleation mechanisms in nanostructured polymer materials and confirming the usefulness of batch foaming processes in producing such materials.

5. Conclusion and perspectives

Polymer foams are already extensively used as insulating materials, but their thermal conductivity remains higher than that of air. Consequently, a further reduction in their thermal conductivity remains an exciting challenge. However, it can be expected the Knudsen effect that appears in nano-cells will provide nano-cellular foams could approach the thermal insulation properties of aerogels. In the preceding, we presented an analytical model of heat transfer in polymer foams based on similar treatments for aerogels. This model predicts in a qualitative way the influence of the foam density and the cell size on the thermal conductivity of polymer foams. Theoretically, this model allowed us to highlight the optimal foam density ($0.1\text{--}0.2 \text{ g cm}^{-3}$) and cell size ($<100 \text{ nm}$) to obtain a polymer foam with an effective thermal conductivity lower than that of air. Moreover, some studies on PEI foams confirmed that nano-cellular materials can have very low thermal conductivities ($<0.02 \text{ W m}^{-1} \text{ K}^{-1}$) because of the Knudsen effect. However, as far as we know, this work is the only one to report thermal conductivity lower than air.

The batch CO₂ foaming process is generally used for the fabrication of homogeneous polymer foams. Two different processes have been investigated:

- a two-stage process where the nucleation is induced by pressure drop quenching after a saturation stage under supercritical conditions. The latter could be longer than a heating stage.
- a two-stage process with thermal quenching to induce cell nucleation and growth after a saturation stage at 'low' temperature under gaseous/supercritical conditions.

For both processes, the fabrication of nano-cellular polymer foams requires the optimization of processing parameters at each stage to ensure cell formation while controlling for the polymer/gas system rheology. The foaming process has to be optimized depending on the CO₂-philic behavior of the polymer and its initial glass transition. In specific cases, the foaming of neat polymers can produce nanocellular foams by means of optimized batch foaming processes. Another way to control the nucleation rate and cell growth is to develop selective foaming and/or preferred heterogeneous nucleation during the foaming process. With this technique, obtaining nanocellular foams with cell size less than 100 nm seems to be difficult and densities of nano-cellular foams are generally higher than 0.2 g cm⁻³. This is because of a nucleation rate that is not significant enough to obtain very low-density materials. Moreover, as reported in Table 8, most studies do not refer to the measurement of foam thermal conductivities. This could reflect the difficulty of performing such measurements on samples too small and too thin.

In all cases, the current challenge in batch CO₂ foaming consists in decreasing the foam densities while keeping cell size less than 100 nm. To that end, nucleation must be applied to increase the cell density to 10¹⁵ cm⁻³. Some studies have shown that the production of foams with cell size less than 100 nm and density between 0.1 and 0.2 g cm⁻³ is possible by combining high homogeneous and heterogeneous nucleation mechanisms in nanostructured polymer materials.

One way to increase nucleation is to combine the effects of different nucleating agents to alter the heterogeneous nucleation phenomenon. The nano-structuration of polymers, via block copolymer or nano-filters, offers a new and original way to fabricate nano-foams with a thermal conductivity lower than that of air. However, some challenges have still to be theoretically and experimentally investigated.

However, the role of polymer viscoelasticity needs to be thoroughly understood because it controls the cell growth and consequently the final density of the foam. It is generally believed that strain hardening is absolutely necessary for the foaming of viscoelastic liquid (foaming at temperature much higher than T_g , process 1). In the case of foaming of temporary viscoelastic gel (foaming at temperature just above T_g , process 2) no specific study is reported in the literature in terms of gel density and consequently in terms of molecular architecture or formulation. Undoubtedly, viscoelasticity, via control of polymer architecture, is the breakthrough needed to develop nano-foaming.

Finally, if some goals can be met by samples obtained on the lab scale, the scale-up of this foaming process to the pilot and industrial scales is another exciting challenge.

Acknowledgements

The authors are grateful to the Hutchinson and Total companies and the Association Nationale Recherche Technologie (ANRT) for the financial support of this work.

References

- [1] Yilmaz Z. Evaluation of energy efficient design strategies for different climatic zones: comparison of thermal performance of buildings in temperate-humid and hot-dry climate. *Energy Build* 2007;39:306–16.
- [2] Choy CL. Thermal conductivity of polymers. *Polymer* 1977;18:984–1004.
- [3] Touloukian YS, Powell RW, Ho CY, Klemens G. Thermophysical properties of matter vol. 2. Thermal conductivity non metallic solids. New York/Washington: IFI/Plenum; 1970, 1302 pp.
- [4] Jannat Y, Degiovanni A. Thermal properties measurement of dry bulk materials with a cylindrical three layers device. *Rev Sci Instrum* 2013;84(094901):1–9.
- [5] Touloukian YS, Liley PE, Saxena SC. Thermophysical properties of matter vol. 3. Thermal conductivity: non metallic liquids and gas. New York/Washington: IFI/Plenum; 1970, 632 pp.
- [6] Danowska M, Piszczyk L, Strankowski M, Gazda M, Haponiuk JT. Rigid polyurethane foams modified with selected layered silicate nanofillers. *J Appl Polym Sci* 2013;130:2272–81.
- [7] Lu X, Caps R, Fricke J, Alviso CT, Pekala RW. Correlation between structure and thermal conductivity of organic aerogels. *J Non Cryst Solids* 1995;188:226–34.
- [8] Connor EF, Lee VY, Magbitang T, Hawker CJ, Volksen W, Siemens R, DiPietro RA, Hedrick JC, Kim HC, Miller RD, Hedrick JL. First example of a nanoporous high-temperature polymer thermoset: eluding transition–time–temperature constraints associated with organic thermosets. *Adv Mater* 2004;16:1525–9.
- [9] Kato T, Hillmyer MA. Functionalized nanoporous polyethylene derived from miscible block polymer blends. *ACS Appl Mater Interfaces* 2013;5:291–300.
- [10] Meyer U, Larsson A, Hentze HP, Caruso RA. Templating of porous polymeric beads to form porous silica and titania spheres. *Adv Mater* 2002;14:1768–72.
- [11] Polarz S, Antonietti M. Porous materials via nanocasting procedures: innovative materials and learning about soft-matter organization. *Chem Commun* 2002;1604–2593.
- [12] Smarsly B, Antonietti M. Block copolymer assemblies as templates for the generation of mesoporous inorganic materials and crystalline films. *Eur J Inorg Chem* 2006;2006:1111–9.
- [13] Hosseini SA, Tafreshi HV. On the importance of fibers' cross-sectional shape for air filters operating in the slip flow regime. *Powder Technol* 2011;212:425–31.
- [14] Lee JH, Grossman JC, Reed J, Galli G. Lattice thermal conductivity of nanoporous Si: molecular dynamics study. *Appl Phys Lett* 2007;91:223110.
- [15] Passian A, Warmack RJ, Wig A, Farahi RH, Meriaudeau F, Ferrell TL, Thundat T. Observation of Knudsen effect with microcantilevers. *Ultramicroscopy* 2003;97:401–6.
- [16] Reglero-Ruiz JA, Saiz-Arroyo C, Dumon M, Rodriguez-Perez MA, Gonzalez L. Production, cellular structure and thermal conductivity of microcellular methyl methacrylate-butyl acrylate-methyl methacrylate triblock copolymers. *Polym Int* 2011;60:146–52.
- [17] Abramenko AN, Kalinichenko AS, Burster Y, Kalinichenko VA, Tanaeva SA, Vasilenko IP. Determination of the thermal conductivity of foam aluminum. *J Eng Phys Thermophys* 1999;72:369–73.
- [18] Collishaw PG, Evans JRG. An assessment of expressions for the apparent thermal conductivity of cellular materials. *J Mater Sci* 1994;29:2261–73.
- [19] Gibson L, Ashby M. Cellular solids. 2nd ed. Cambridge: Cambridge University Press; 1997, 510 pp.
- [20] Baetens R, Jelle BrP, Gustavsen A. Aerogel insulation for building applications: a state-of-the-art review. *Energy Build* 2011;43:761–9.
- [21] Fricke J, Hummer E, Morper H, Scheuerpfugl P. Thermal properties of silica aerogels. *J Phys Colloq* 1989;50:C4–87.

- [22] Hrubesh LW, Pekala RW. Thermal properties of organic and inorganic aerogels. *J Mater Res* 1994;9:731–8.
- [23] Kumar V, Suh NP. A process for making microcellular thermoplastic parts. *Polym Eng Sci* 1990;30:1323–9.
- [24] Costeux S, Zhu L. Low density thermoplastic nanofoams nucleated by nanoparticles. *Polymer* 2013;54:2785–95.
- [25] Sundaram SS, Li W. On thermal conductivity of micro and nanocellular polymer foams. *Polym Eng Sci* 2013;53:1901–9.
- [26] Sorrentino L, Aurilia M, Iannace S. Polymeric foams from high-performance thermoplastics. *Adv Polym Technol* 2001;30:234–43.
- [27] Luo Y, Ye C. Using nanocapsules as building blocks to fabricate organic polymer nanofoam with ultra low thermal conductivity and high mechanical strength. *Polymer* 2012;53:5699–705.
- [28] Kumar V. Microcellular polymers: novel materials for the 21st century? *Cell Polym* 1993;12:207–23.
- [29] Saucet M, Fages J, Common A, Nikitine C, Rodier E. New challenges in polymer foaming: a review of extrusion processes assisted by supercritical carbon dioxide. *Prog Polym Sci* 2011;36:749–66.
- [30] Tomasko DL, Li H, Liu D, Han X, Wingert MJ, Lee LJ, Koelling KW. A review of CO₂ applications in the processing of polymers. *Ind Eng Chem Res* 2003;42:6431–56.
- [31] Guevara-Rodriguez FdJ, Romero-Martinez A. An empirical extension for a generalized cubic equation of state, applied to a pure substance with small molecules. *Fluid Phase Equilib* 2013;347:22–7.
- [32] Walker TA, Frankowski DJ, Spontak RJ. Thermodynamics and kinetic processes of polymer blends and block copolymers in the presence of pressurized carbon dioxide. *Adv Mater* 2008;20:879–98.
- [33] Klopffer MH, Flaconneche B. Transport properties of gases in polymers: bibliographic review. *Oil Gas Sci Tech Rev IFP* 2001;56:223–44.
- [34] Miller D, Chatchaisucha P, Kumar V. Microcellular and nanocellular solid-state polyetherimide (PEI) foams using sub-critical carbon dioxide I. Processing and structure. *Polymer* 2009;50:5576–84.
- [35] Handa YP, Zang Z, Wong B. Solubility, diffusivity, and retrograde vitrification in pmma-CO₂, and development of sub-micron cellular structures. *Cell Polym* 2001;20:1–16.
- [36] Marchese J, Garis E, Anson M, Ochoa M, Pagliero C. Gas sorption, permeation and separation of abs copolymer membrane. *J Membr Sci* 2003;221:185–97.
- [37] Pantoula M, Panayiotou C. Sorption and swelling in glassy polymer/carbon dioxide systems. Part I. Sorption. *J Supercrit Fluids* 2006;37:254–62.
- [38] Vitoux P, Tassaing T, Cansell F, Marre S, Aymonier C. In situ ir spectroscopy and ab initio calculations to study polymer swelling by supercritical CO₂. *J Phys Chem B* 2009;113:897–905.
- [39] Neogi P, editor. *Diffusion in polymer*. Boca Raton, FL: CRC Press; 1996, 328 pp.
- [40] Cohen MH, Turnbull D. Molecular transport in liquids and glasses. *J Chem Phys* 1959;31:1164–9.
- [41] Vrentas JS, Duda JL. Diffusion in polymer–solvent systems. I. Reexamination of the free-volume theory. *J Polym Sci Part B Polym Phys* 1997;35:403–16.
- [42] Vrentas JS, Vrentas CM. Solvent self-diffusion in glassy polymer-solvent systems. *Macromolecules* 1994;27:5570–6.
- [43] Vrentas JS, Vrentas CM. Solvent self-diffusion in rubbery polymer-solvent systems. *Macromolecules* 1994;27:4684–90.
- [44] Naito Y, Kamiya Y, Terada K, Mizoguchi K, Wang JS. Pressure dependence of gas permeability in a rubbery polymer. *J Appl Polym Sci* 1996;61:945–50.
- [45] Chen X, Feng JJ, Bertelo CA. Plasticization effects on bubble growth during polymer foaming. *Polym Eng Sci* 2006;46:97–107.
- [46] Ferry JD. *Viscoelastic properties of polymers*. 2nd ed. New York: John Wiley & Sons Inc.; 1970, 671 pp.
- [47] Hachisuka H, Sato T, Imai T, Tsujita Y, Takizawa A, Kinoshita T. Glass transition temperature of glassy polymers plasticized by CO₂ gas. *Polym J* 1990;22:77–9.
- [48] Wissinger RG, Paulaitis ME. Glass transitions in polymer/CO₂ mixtures at elevated pressures. *J Polym Sci Part B Polym Phys* 1991;29:631–3.
- [49] Kamiya Y, Mizoguchi K, Naito Y. A dielectric-relaxation study of plasticization of poly(ethyl methacrylate) by carbon-dioxide. *J Polym Sci Part B Polym Phys* 1990;28:1955–64.
- [50] Houde AY, Kulkarni SS, Kulkarni MG. Permeation and plasticization behavior of glassy-polymers – a waxd interpretation. *J Membr Sci* 1992;71:117–28.
- [51] Zhang Z, Handa YP. An in situ study of plasticization of polymers by high-pressure gases. *J Polym Sci Part B Polym Phys* 1998;36:977–82.
- [52] Handa P, Zhang Z. A new technique for measuring retrograde vitrification in polymer-gas systems and for making ultramicrocellular foams from the retrograde phase. *J Polym Sci Part B Polym Phys* 2000;38:716–25.
- [53] Nawaby AV, Handa YP, Liao X, Yoshitaka Y, Tomohiro M. Polymer-CO₂ systems exhibiting retrograde behavior and formation of nanofoams. *Polym Int* 2007;56:67–73.
- [54] Doolittle AK. Studies in Newtonian flow. 1. The dependence of the viscosity of liquids on temperature. *J Appl Phys* 1951;22:1031–5.
- [55] Chow TS. Molecular interpretation of the glass-transition temperature of polymer-diluent systems. *Macromolecules* 1980;13:362–4.
- [56] Dong Hwang Y, Woon Cha S. The relationship between gas absorption and the glass transition temperature in a batch microcellular foaming process. *Polym Test* 2002;21:269–75.
- [57] Yoon JD, Cha SW. Change of glass transition temperature of polymers containing gas. *Polym Test* 2001;20:287–93.
- [58] Condo PD, Johnston KP. Retrograde vitrification of polymers with compressed fluid diluents: experimental confirmation. *Macromolecules* 1992;25:6730–2.
- [59] Condo PD, Johnston KP. In situ measurement of the glass transition temperature of polymers with compressed fluid diluents. *J Polym Sci Part B Polym Phys* 1994;32:523–33.
- [60] Tsioptisias C, Panayiotou C. Simultaneous determination of sorption, heat of sorption, diffusion coefficient and glass transition depression in polymer-CO₂ systems. *Thermochim Acta* 2011;521:98–106.
- [61] Manninen AR, Naguib HE, Nawaby AV, Day M. CO₂ sorption and diffusion in polymethyl-methacrylate-clay nanocomposites. *Polym Eng Sci* 2005;45:904–14.
- [62] Tang Q, Yang B, Zhao Y, Zhao L. Sorption and diffusion of sub/supercritical carbon dioxide in poly(methyl methacrylate). *J Macromol Sci Part B* 2007;46:275–84.
- [63] Dutriez C, Satoh K, Kamigaito M, Yokoyama H. Nanocellular foaming of fluorine containing block copolymers in carbon dioxide: the role of glass transition in carbon dioxide. *RSC Adv* 2012;2:2821–7.
- [64] Reglero-Ruiz JA, Viot P, Dumon M. Foaming of amorphous polymers and blends in supercritical CO₂: solubility versus block copolymers addition. *J Cell Plast* 2011;47:535–48.
- [65] Williams LL, Rubin JB, Edwards HW. Calculation of Hansen solubility parameter values for a range of pressure and temperature conditions, including the supercritical fluid region. *Ind Eng Chem Res* 2004;43:4967–72.
- [66] Flory PJ. *Principles of polymer chemistry*. Ithaca NY: Cornell University Press; 1953, 672 pp.
- [67] Hildebrand JH, Scott RL. *The solubility of nonelectrolytes*. 3rd ed. New York: Reinhold; 1950, 488 pp.
- [68] Gupta R, Shim J. Solubility in supercritical carbon dioxide. Boca Raton, FL: CRC Press; 2006, 909 pp.
- [69] Strauss W, D'Souza NA. Supercritical CO₂ processed polystyrene nanocomposite foams. *J Cell Plast* 2004;40:229–41.
- [70] Garcia-Leiner M, Lesser AJ. CO₂-assisted polymer processing: a new alternative for intractable polymers. *J Appl Polym Sci* 2004;93:1501–11.
- [71] Kazarian SG, Vincent MF, Bright FV, Liotta CL, Eckert CA. Specific intermolecular interaction of carbon dioxide with polymers. *J Am Chem Soc* 1996;118:1729–36.
- [72] Hansen CM. Aspects of solubility, surfaces, and diffusion in polymers. *Prog Org Coat* 2004;51:55–66.
- [73] Hansen CM. Hansen solubility parameters. Boca Raton, FL: CRC Press; 2002, 208 pp.
- [74] Kasturirangan A, Koh CA, Teja AS. Glass-transition temperatures in CO₂ + polymer systems: modeling and experiment. *Ind Eng Chem Res* 2011;50:158–62.
- [75] André P, Lacroix-Desmazes P, Taylor DK, Boutevin B. Solubility of fluorinated homopolymer and block copolymer in compressed CO₂. *J Supercrit Fluids* 2006;37:263–70.
- [76] Ribaut T, Oberdisse J, Annighofer B, Fournel B, Sarrade S, Haller H, Lacroix-Desmazes P. Solubility and self-assembly of amphiphilic gradient and block copolymers in supercritical CO₂. *J Phys Chem B* 2011;115:836–43.
- [77] Kilic S, Michalik S, Wang Y, Johnson JK, Beckman Ej, Enick RM. Phase behavior of oxygen-containing polymers in CO₂. *Macromolecules* 2007;40:1332–41.
- [78] Cooper Al. Polymer synthesis and processing using supercritical carbon dioxide. *J Mater Chem* 2000;10:207–34.

- [79] Fink R, Hancu D, Valentine R, Beckman EJ. Toward the development of CO₂-philic hydrocarbons. I: use of side-chain functionalization to lower the miscibility pressure of polydimethylsiloxanes in CO₂. *J Phys Chem B* 1999;103:6441–4.
- [80] Kilic S, Wang Y, Johnson JK, Beckman EJ, Enick RM. Influence of tert-amine groups on the solubility of polymers in CO₂. *Polymer* 2009;50:2436–44.
- [81] Kirby CF, McHugh MA. Phase behavior of polymers in supercritical fluid solvents. *Chem Rev* 1999;99:565–602.
- [82] Nalawade SP, Picchioni F, Janssen LPBM. Supercritical carbon dioxide as a green solvent for processing polymer melts: processing aspects and applications. *Prog Polym Sci* 2006;31:19–43.
- [83] Fried JR, Li W. High-pressure FTIR studies of gas-polymer interactions. *J Appl Polym Sci* 1990;41:1123–31.
- [84] Shieh YT, Liu KH. The effect of carbonyl group on sorption of CO₂ in glassy polymers. *J Supercrit Fluids* 2003;25:261–8.
- [85] Gibbs JW. The scientific papers of J. Willard Gibbs volume 1. New York: Dover Publications Inc.; 1961, 434 pp.
- [86] Wong A, Guo Q, Park CB. Fundamental mechanisms of cell nucleation in polypropylene foaming with supercritical carbon dioxide: effects of extensional stresses and crystals. *J Supercrit Fluids* 2013;79:142–51.
- [87] Leung SN, Wong A, Guo Q, Park CB, Zong JH. Change in the critical nucleation radius and its impact on cell stability during polymeric foaming processes. *Chem Eng Sci* 2009;64:4899–907.
- [88] Krause B, Sijbesma HJP, Munukutla P, Van Der Vegt NFA, Wessling M. Bicontinuous nanoporous polymers by carbon dioxide foaming. *Macromolecules* 2001;34:8792–801.
- [89] Costeux S, Bunker SP, Jeon HK. Homogeneous nanocellular foams from styrenic-acrylic polymer blends. *J Mater Res* 2013;28:2351–65.
- [90] Otsuka T, Taki K, Ohshima M. Nanocellular foams of PS/PMMA polymer blends. *Macromol Mater Eng* 2008;293:78–82.
- [91] Reglero-Ruiz JA, Pedros M, Tallon JM, Dumon M. Micro and nano cellular amorphous polymers (PMMA, PS) in supercritical CO₂ assisted by nanostructured CO₂-philic block copolymers – one step foaming process. *J Supercrit Fluids* 2011;58:168–76.
- [92] Mahmoodi M, Behravesh AH. The effect of pressure drop rate on microstructure of unfilled and glass-filled abs microcellular foams. *Iran Polym J* 2007;16:839–49.
- [93] Leung SN, Wong A, Park CB, Guo Q. Strategies to estimate the pressure drop threshold of nucleation for polystyrene foam with carbon dioxide. *Ind Eng Chem Res* 2009;48:1921–7.
- [94] Famili MHN, Janani H, Enayati MS. Foaming of a polymer-nanoparticle system: effect of the particle properties. *J Appl Polym Sci* 2011;119:2847–56.
- [95] Goren K, Chen L, Schadler LS, Ozisik R. Influence of nanoparticle surface chemistry and size on supercritical carbon dioxide processed nanocomposite foam morphology. *J Supercrit Fluids* 2010;51:420–7.
- [96] Wong A, Wijnands SFL, Kuboki T, Park CB. Mechanisms of nanoclay-enhanced plastic foaming processes: effects of nanoclay intercalation and exfoliation. *J Nanopart Res* 2013;15:1815–15.
- [97] Kim Y, Park CB, Chen P, Thompson RB. Origins of the failure of classical nucleation theory for nanocellular polymer foams. *Soft Matter* 2011;7:7351–8.
- [98] Xu X, Cristancho DE, Costeux S, Wang ZG. Bubble nucleation in polymer-CO₂ mixtures. *Soft Matter* 2013;9:9675–83.
- [99] Xu X, Cristancho DE, Costeux S, Wang ZG. Discontinuous bubble nucleation due to a metastable condensation transition in polymer CO₂ mixtures. *J Phys Chem Lett* 2013;4:1639–43.
- [100] Shafi M, Flumerfelt RW. Initial bubble growth in polymer foam processes. *Chem Eng Sci* 1997;52:627–33.
- [101] Shafi MA, Joshi K, Flumerfelt RW. Bubble size distributions in freely expanded polymer foams. *Chem Eng Sci* 1997;52:635–44.
- [102] Liao R, Yu W, Zhou C. Rheological control in foaming polymeric materials: II. Semi-crystalline polymers. *Polymer* 2010;51:6334–45.
- [103] Zhai W, Wang J, Chen N, Naguib HE, Park CB. The orientation of carbon nanotubes in poly(ethylene-co-octene) microcellular foaming and its suppression effect on cell coalescence. *Polym Eng Sci* 2012;52:2078–89.
- [104] Li S, Xiao M, Guan Y, Wei D, Xiao H, Zheng A. A novel strategy for the preparation of long chain branching polypropylene and the investigation on foamability and rheology. *Eur Polym J* 2012;48:362–71.
- [105] Matuana LM, Diaz CA. Study of cell nucleation in microcellular poly(lactic acid) foamed with supercritical CO₂ through a continuous extrusion process. *Ind Eng Chem Res* 2010;49:2186–93.
- [106] Mihai M, Huneault MA, Favis BD. Rheology and extrusion foaming of chain-branched poly(lactic acid). *Polym Eng Sci* 2010;50:629–42.
- [107] Otsuki Y, Kanai T. Numerical simulation of bubble growth in viscoelastic fluid with diffusion of dissolved foaming agent. *Polym Eng Sci* 2005;45:1277–87.
- [108] McCallum TJ, Kontopoulou M, Park CB, Wong A, Kim SG. Effect of branched pp content on the physical properties and cell growth during foaming of tpos. *J Appl Polym Sci* 2008;110:817–24.
- [109] Liao R, Yu W, Zhou C. Rheological control in foaming polymeric materials: I. Amorphous polymers. *Polymer* 2010;51:568–80.
- [110] Stafford CM, Russell TP, McCarthy TJ. Expansion of polystyrene using supercritical carbon dioxide: effects of molecular weight, polydispersity and low molecular weight components. *Macromolecules* 1999;32:7610–6.
- [111] Yokoyama H, Sugiyama K. Nanocellular structures in block copolymers with CO₂-philic blocks using CO₂ as a blowing agent: crossover from micro- to nanocellular structures with depressurization temperature. *Macromolecules* 2005;38:10516–22.
- [112] Krause B, Diekmann K, Van Der Vegt NFA, Wessling M. Open nanoporous morphologies from polymeric blends by carbon dioxide foaming. *Macromolecules* 2002;35:1738–45.
- [113] Sandler JKW, Francis T, Manuel P, Lopes S. Nanoporous polymer foams. *US* 20110287260 A1; 2011.
- [114] Janani H, Famili MHN. Investigation of a strategy for well controlled induction of microcellular and nanocellular morphologies in polymers. *Polym Eng Sci* 2010;50:1558–70.
- [115] Taki K, Waratani Y, Ohshima M. Preparation of nanowells on a PS-B-PMMA copolymer thin film by CO₂ treatment. *Macromol Mater Eng* 2008;293:589–97.
- [116] Li L, Yokoyama H, Nemoto T, Sugiyama K. Facile fabrication of nanocellular block copolymer thin films using supercritical carbon dioxide. *Adv Mater* 2004;16:1226–9.
- [117] Yokoyama H, Li L, Nemoto T, Sugiyama K. Tunable nanocellular polymeric monoliths using fluorinated block copolymer templates and supercritical carbon dioxide. *Adv Mater* 2004;16:1542–6.
- [118] Zhang R, Dutriez C, Sugiyama K, Ishizone T, Yokoyama H. Thermally robust nanocellular thin films of high-(g) semifluorinated block copolymers foamed with supercritical carbon dioxide. *Soft Matter* 2001;7:4032–8.
- [119] Reglero-Ruiz JA, Cloutet E, Dumon M. Investigation of the nanocellular foaming of polystyrene in supercritical CO₂ by adding a CO₂-philic perfluorinated block copolymer. *J Appl Polym Sci* 2012;126:38–45.
- [120] Sorrentino L, Aurilia M, Cafiero L, Iannace1 S. Nanocomposite foams from high-performance thermoplastics. *J Appl Polym Sci* 2011;122:3701–10.
- [121] Ito Y, Yamashita M, Okamoto M. Foam processing and cellular structure of polycarbonate-based nanocomposites. *Macromol Mater Eng* 2006;291:773–83.
- [122] Martinez AB, Realinho V, Antunes M, Maspoch ML, Velasco JL. Microcellular foaming of layered double hydroxide polymer nanocomposites. *Ind Eng Chem Res* 2011;50:5239–47.
- [123] Realinho V, Antunes M, Martinez AB, Velasco JL. Influence of nanoclay concentration on the CO₂ diffusion and physical properties of PMMA montmorillonite microcellular foams. *Ind Eng Chem Res* 2011;50:13819–24.
- [124] Siripurapu S, DeSimone JM, Khan SA, Spontak RJ. Controlled foaming of polymer films through restricted surface diffusion and the addition of nanosilica particles or CO₂-philic surfactants. *Macromolecules* 2005;38:2271–80.
- [125] Zhai W, Yu J, Wu L, Ma W, He J. Heterogeneous nucleation uniformizing cell size distribution in microcellular nanocomposites foams. *Polymer* 2006;47:7580–9.
- [126] Takahashi T, Wu W, Toda H, Takimoto JL, Akatsuka T, Koyama K. Elongational viscosity of abs polymer melts with soft or hard butadiene particles. *J Non Newtonian Fluid Mech* 1997;68:259–69.
- [127] Holl MR, Kumar V, Garbini JL, Murray WR. Cell nucleation in solid-state polymeric foams: evidence of a triaxial tensile failure mechanism. *J Mater Sci* 1999;34:637–44.
- [128] Murray RE, Weller JE, Kumar V. Solid-state microcellular acrylonitrile-butadiene-styrene foams. *Cell Polym* 2000;19:413–25.
- [129] Nemoto T, Takagi J, Ohshima M. Nanoscale cellular foams from a poly(propylene)-rubber blend. *Macromol Mater Eng* 2008;293:991–8.
- [130] Spitael P, Macosko CW, McClurg RB. Block copolymer micelles for nucleation of microcellular thermoplastic foams. *Macromolecules* 2004;37:6874–8682.

- [131] Dumon M, Reglero-Ruiz JA, Pinto-Sanz J, Rodriguez Perez MA, Tallon JM, Pedros M, Clouet E, Viot P. Block copolymer-assisted microcellular supercritical CO₂ foaming of polymers and blends. *Cell Polym* 2012;31:207–22.
- [132] Reglero-Ruiz JA, Tallon JM, Pedros M, Dumon M. Two-step micro cellular foaming of amorphous polymers in supercritical CO₂. *J Supercrit Fluids* 2011;57:87–94.
- [133] Reglero-Ruiz JA, Viot P, Dumon M. Microcellular foaming of poly-methylmethacrylate in a batch supercritical CO₂ process: effect of microstructure on compression behavior. *J Appl Polym Sci* 2010;118:320–31.
- [134] Reglero-Ruiz JA, Dumon M, Pinto-Sanz J. Low-density nanocellular foams produced by high-pressure carbon dioxide. *Macromol Mater Eng* 2011;296:752–9.